# Investigation of the Determinants of Agonism in a Ligand-Gated Ion Channel using Statistical Coupling Analysis

Mykhaylo Slobodyanyuk

A thesis submitted in partial fulfillment of the requirements for the M.Sc. degree in Chemistry

Department of Chemistry and Biomolecular Sciences

Faculty of Science

University of Ottawa

Ottawa, Canada

# Abstract

The prokaryotic *Erwinia chrysanthemi* ligand-gated ion channel (ELIC) is competitively inhibited by acetylcholine (Pan et al., 2012). Acetylcholine is the native agonist of the structurally related family of eukaryotic acetylcholine receptors, which like ELIC are pentameric ligand-gated ion channels. To understand the opposite effect upon acetylcholine binding between ELIC and acetylcholine receptors, we used statistical coupling analysis to predict mutations necessary for installing acetylcholine agonism into ELIC. Statistical coupling analysis was performed on the acetylcholine binding protein from *Lymnaea stagnalis*. This protein is a structural surrogate for the agonist binding domain of acetylcholine receptors, for which a high-resolution structure in complex with acetylcholine is available. Our analysis identified a group of statistically coupled residues that comprises several amino acids previously implicated in acetylcholine agonism of acetylcholine receptors. Mapping these residues onto ELIC revealed 15 residue discrepancies, 4 of which were chosen for initial mutagenesis based upon their proximity to the known agonist binding site. Electrophysiological characterization of ELIC mutants indicates that the potency of the native agonist, cysteamine, is decreased, highlighting the optimized role wild-type residues serve in native agonism. None of the mutants were activated by acetylcholine, however the double mutant A75D/F133W abolished competitive antagonism by acetylcholine, and instead led to acetylcholine dependent potentiation of cysteamine-induced currents. This work demonstrates the ability of statistical coupling analysis to identify functionally important residues in pentameric ligand-gated ion channels and reveals that acetylcholine can be converted from a competitive antagonist into a potentiator, by installing two residues present in acetylcholine receptors.

# Acknowledgements

I want to express my gratitude to everyone that helped me along the journey in graduate school and for the invaluable conversations, insight and guidance that you all provided.

I'd like to thank my co-supervisor Dr. Roberto Chica. Thank you for the incredibly detailed and thorough help you provided me in preparing presentations, abstracts and posters. You have instilled the importance of good scientific communication in all of us and for that I am grateful!

To my co-supervisor Dr. Corrie daCosta, thank you for inspiring me to pursue Biochemistry in graduate school with your passionate and informative lectures. I admire the rigor with which you approach problems and the incredible knowledge and passion you have for the field. I'm grateful to have had the opportunity to work with you!

To Dr. Jesús Agustín Banda-Vázquez, your insight and determination throughout my graduate studies were invaluable to the completion of this project. From the idea of the project, to the computational work and data analysis, this project couldn't have been completed without you. It was a pleasure working with you!

To my lab members, you've all been so inspiring to me and have helped me grow as a scientist. I'd like to thank, in no particular order: Mathew Eason, Tony St-Jacques, Adam Damry, Greg McCluskey, Johnathon Emlaw, Christian Tessier, Sandrine Legault, Rojo Rakotoharisoa, Abdel Rahman Lepabic, Niayesh Zarifi and Marc Mayer.

I'd also like to thank Dr. John Baenziger for your insights and your generosity in allowing me use of your lab and equipment to gather most of the data in this thesis! To Mackenzie Thompson, thank you for preparing the oocytes each week and for the enlightening conversations that have helped me understand this field much better than before I started!

To my parents, for their unwavering support and interest in anything I do. Thank you for nudging me on to pursue this challenging but rewarding degree. I couldn't have done this without you!

# Table of Contents

# List of Abbreviations

| | |
|---|---|
| 5-AV | 5-aminovaleric acid |
| $5HT_3$-R | Serotonin receptor |
| ΔG | Gibbs free energy change |
| pLGIC | Pentameric ligand-gated ion channel |
| ACh | Acetylcholine |
| AChBP | Acetylcholine binding protein |
| $Ca^{2+}$ | Calcium ion |
| CD | Cytoplasmic domain |
| $CO_2$ | Carbon dioxide |
| cRNA | Capped ribonucleic acid |
| Cryo-EM | Cryogenic-electron microscopy |
| DMAEA | 2-methylaminoethylacetate |
| DTT | Dithiothreitol |
| $EC_{50}$ | Half maximal effective concentration |
| ECD | Extracellular domain |
| ELIC | *Erwinia chrysanthemi* ligand-gated ion channel |
| $GABA_AR$ | Gamma-aminobutyric acid receptor |
| GBH | Gamma-hydroxybutyric acid |
| GLIC | *Gloeobacter violaceus* ligand-gated ion channel |
| GluClR | Glutamate-gated chloride receptor |
| GlyR | Glycine receptor |
| HEPES | 4-(2-hydroxyethyl)-1-piperazineethanesulfonic acid |
| HMM | Hidden Markov Model |

| | |
|---|---|
| ICD | Intracellular domain |
| $K^+$ | Potassium ion |
| kDa | Kilodaltons |
| LGIC | Ligand-gated ion channel |
| M1 | Transmembrane α-helix 1 |
| M2 | Transmembrane α-helix 2 |
| M3 | Transmembrane α-helix 3 |
| M4 | Transmembrane α-helix 4 |
| m | Mutation |
| MA | Intracellular α-helix A |
| MSA | Multiple sequence alignment |
| MWC | Monod-Wyman-Changeux |
| MX | Intracellular α-helix X |
| $Na^+$ | Sodium ion |
| nAChR | Nicotinic acetylcholine receptor |
| PCR | Polymerase chain reaction |
| PDB | Protein data bank |
| RBS | Ribose buffered saline |
| SCA | Statistical coupling analysis |
| TEVC | Two-electrode voltage clamp |
| TMD | Transmembrane domain |
| WT | Wild-type |

# List of Figures

### Chapter 1 - Introduction



### Chapter 2 – Experimental Procedures



### Chapter 3 - Results



### Appendix

# List of Tables

# Chapter 1 – Introduction

## 1.1 Ligand-Gated Ion Channels

Cells are the basic units of life that through billions of years of evolution have developed coordinated and complex systems to respond to different external stimuli. At the interface of this extracellular stimulus, whether it be light, heat, pressure, voltage, or a chemical, are integral membrane proteins called receptors. These receptors serve as both a means of detecting and transducing external signals, which can trigger the activation of cellular pathways. An important class of integral membrane receptors are ligand-gated ion channels (LGIC). These bind a variety of molecules such as ions, lipids, polypeptides, drugs, and neurotransmitters; only a select few of these molecules have the capacity to activate the channel. The binding of a specific ligand triggers a conformational change in the receptor that enables the channel pore to open, allowing for the selective permeation of ions across a lipid membrane on the millisecond timescale. These ions subsequently cause the depolarization or hyperpolarization of the cell, which leads to a variety of functions, such as cellular communication. The LGICs are divided into trimeric, tetrameric and pentameric assemblies, composing P2X receptors, glutamate receptors, and pentameric ligand-gated ion channels (pLGICs), respectively. Of these three families, the pLGICs are the most prominent and diverse (Alexander et al., 2011).

## 1.2 Eukaryotic vs Prokaryotic pLGICs

The focus of this thesis is on the prokaryotic *Erwinia chrysanthemi* ligand-gated ion channel (ELIC), a member of the pLGIC superfamily. All members of this superfamily are ionotropic integral membrane receptors composed of five subunits that arrange around a central symmetrical axis, which delineates the ion conduction path (Figure 1.2A). Each subunit is composed of a N-terminal extracellular domain (ECD), responsible for ligand binding, and a transmembrane domain (TMD), responsible for ion conductance and channel gating. Eukaryotic channels also possess a cytoplasmic domain (CD), composed of an amphipathic α-helix, that plays a role in pentameric assembly and conduction of ions (Thompson et al., 2010). Upon binding of an agonist, an extracellular ligand that can activate the receptor, the TMD gate opens to allow ions to flow down their electrochemical gradient.

The pLGICs are categorized by the type of ions they conduct. Excitatory receptors conduct cations such as sodium, potassium and calcium ions, while inhibitory receptors conduct anions such as chloride. Further categorization is based on the agonist that binds and activates these receptors. The nicotinic acetylcholine receptor (nAChR) and serotonin receptor ($5HT_3$-R) are excitatory cation-conducting receptors that bind to and are activated by acetylcholine (ACh) and serotonin, respectively. Inhibitory anion-conducting receptors include the γ-aminobutyric acid type A receptor ($GABA_AR$), glycine receptor (GlyR), and glutamate-gated chloride receptor (GluClR), and bind to and are activated by γ-aminobutyric acid (GABA), glycine, and glutamate, respectively. In 2005, prokaryotic homologs of pLGICs were discovered, demonstrating that this scaffold is ancient and found in almost all forms of life (Tasneem et al., 2005). These prokaryotic pLGICs have a large diversity in architecture and are named according to the genus of the organism they were discovered in. The two best characterized prokaryotic receptors are the

*Gloeobacter violaceus* (GLIC) and *Erwinia chrysanthemi* (ELIC) ligand-gated ion channels. These channels share the highest sequence similarity to their eukaryotic counterparts, making them excellent model systems for understanding the mechanisms of pLGIC function. Unlike their eukaryotic counterparts, ELIC and GLIC are more amenable to X-ray crystallography, and accordingly, structures of both receptors have been solved at 3.3 Å and 2.9 Å resolution, respectively (Hilf and Dutzler, 2008; Bocquet et al., 2009; Hilf and Dutzler, 2009).

Agonist binding to both eukaryotic and prokaryotic pLGICs is done via a set of key contacts between the small molecule and the receptor. These key contacts induce a conformational change that is responsible for ion conduction upon agonist binding. The ability of a molecule to bind and activate pLGICs involves a group of amino acid residues that directly contact the agonist in the binding site, as well as distal residues that link binding to channel gating. This property is highlighted with the neurotransmitter ACh, which is the defining agonist of the nAChR subfamily. Interestingly, ACh binds to ELIC in a similar binding pose and with comparable affinity to those of its endogenous agonists (e.g., GABA), but, uniquely, it functions as a competitive inhibitor. Binding of acetylcholine stabilizes ELIC in a conformational state described as being “on the verge of activation”, with a 1.32 Å widening of the channel pore at its narrowest constriction, which is insufficient to activate the receptor for ion permeation (Pan et al., 2012). The mechanism by which the binding of a small molecule activates an ion channel, an essential component of understanding channel function, has not been well-characterized.

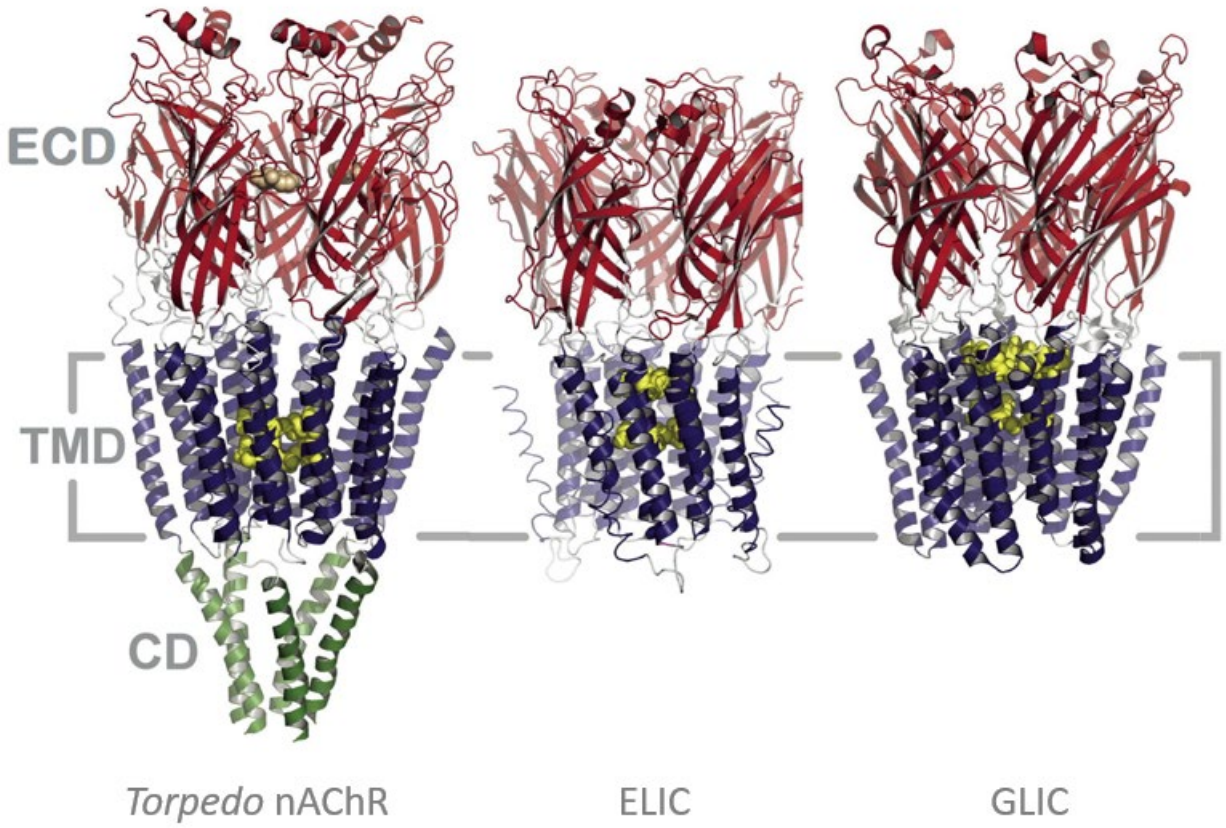


**Figure 1.1 Structure of the *Torpedo* nAChR and homologous prokaryotic ELIC and GLIC pLGICs.**

On the left is a side view of the nAChR (PDB: 2BG9) from the plane of the membrane (depicted in square brackets []), displaying from top to bottom the extracellular domain (ECD, red), transmembrane domain (TMD, blue) and cytoplasmic domain (CD, green). Additionally, tan spheres (αW149 side chains) in the ECD highlight part of the agonist-binding site, and yellow spheres (αL251 and αV255 and analogous residue side chains in the other subunits) in the TMD highlight the channel gate. In the middle, a side view of ELIC (PDB: 2VL0) from the plane of the membrane is displayed and coloured identically to nAChR, with the yellow spheres in the TMD highlighting the channel gate (L239 and F246). On the right, a side view of GLIC (PDB: 4HFI) from the plane of the membrane is displayed and coloured identically to nAChR, with the yellow spheres in the TMD highlighting the channel gate (I233, I240 and L241). Both GLIC and ELIC lack a CD. Figure was reprinted from Structure, 21, daCosta, C. J. B., and Baenziger, J. E., Gating of pentameric ligand-gated ion channels: Structural insights and ambiguities, 1271-1283., 2013, with permission from Elsevier.

## 1.3 The Acetylcholine Binding Protein

Our understanding of pLGICs structure and function, such as ligand binding, channel gating and ion selectivity, have been limited by the difficulty of attaining high resolution x-ray and/or cryo-EM structures of each member in its three general conformations. The first high resolution structural insight into the pLGIC ECD was from the discovery of acetylcholine binding proteins (AChBPs), which are water soluble homopentameric proteins that are homologous to the nAChR ECD (Smit et al., 2001; Figure 1.2). More specifically, crystal structures of AChBP at 2 to 3.4 Å resolution have provided a wealth of information about the residues involved, as well as structural changes affecting the ECD upon agonist binding (Brejc et al., 2001; Hansen et al., 2005). Whilst they themselves lack a TMD for ion conductance, AChBPs undergo a conformational change upon acetylcholine binding that, when linked to the TMD of a 5-$HT_{3A}$ receptor, triggers the opening of the ion pore (Bouzat et al., 2004).

## 1.4 ECD and Agonist Binding

The agonist binding site is located at the interface between two subunits in the ECD (Figure 1.2A-B). In homopentameric proteins such as ELIC, the α7 nAChR, and AChBP, each subunit contributes the principal and complementary face providing a total of five binding sites. An agonist can potentially occupy all these orthosteric sites simultaneously, however this is not a prerequisite for full channel activation (Andersen et al., 2013).

Each subunit is composed of a short N-terminal α helix in the AChBP and nAChR, which is lacking in ELIC. Next, a β sandwich is formed by an inner beta sheet composed of six strands (β1, β2, β3, β5, β6 and β8), and an outer beta sheet composed of four strands (β4, β7, β9 and

β10) (Figure 1.2C). The principal face of the agonist binding site is composed of loop A, B, and C, which are situated between β3-β4, β7-β8, and β9-β10, respectively. These loops form an aromatic box around the quaternary amine neurotransmitters that bind nAChRs and AChBPs, responsible for cation-π interactions (Xiu et al., 2009) and hydrogen bonding interactions (Hansen et al., 2005). In ELIC, conserved aromatic residues surround a similar pocket in volume, which is why it was initially postulated to be opened by ligands of similar size and chemical composition (Hilf and Dutzler, 2008). The complementary face is composed of loops D, E, and F, which correspond to β strands 2, 5 and β8-β9, respectively. The residues on the complementary face tend to vary in composition and are generally thought to contribute to agonist specificity and/or affinity. An identifier of α subunits is the presence of a key vicinal disulfide between cysteine residues in the C-loop of nAChRs and AChBPs (Kao and Karlin, 1986). These cysteine residues and the corresponding vicinal disulfide is absent in ELIC. The C-loop not only contributes key residues for agonist binding, but displays the largest change in conformation in the agonist binding site. In one state, the loop is in a flexible "open" conformation allowing molecules to diffuse into the binding site, and upon binding, adopts a stable "closed" conformation that acts as a cap, effectively trapping the ligand (Taylor et al., 2007; Li et al., 2011; Pan et al., 2012).

Whilst the AChBP subunits terminate at the $10^{th}$ β strand of the ECD, the nAChR and ELIC transition to an M1 α-helix, which is embedded in the plasma membrane, marking the beginning of the TMD.

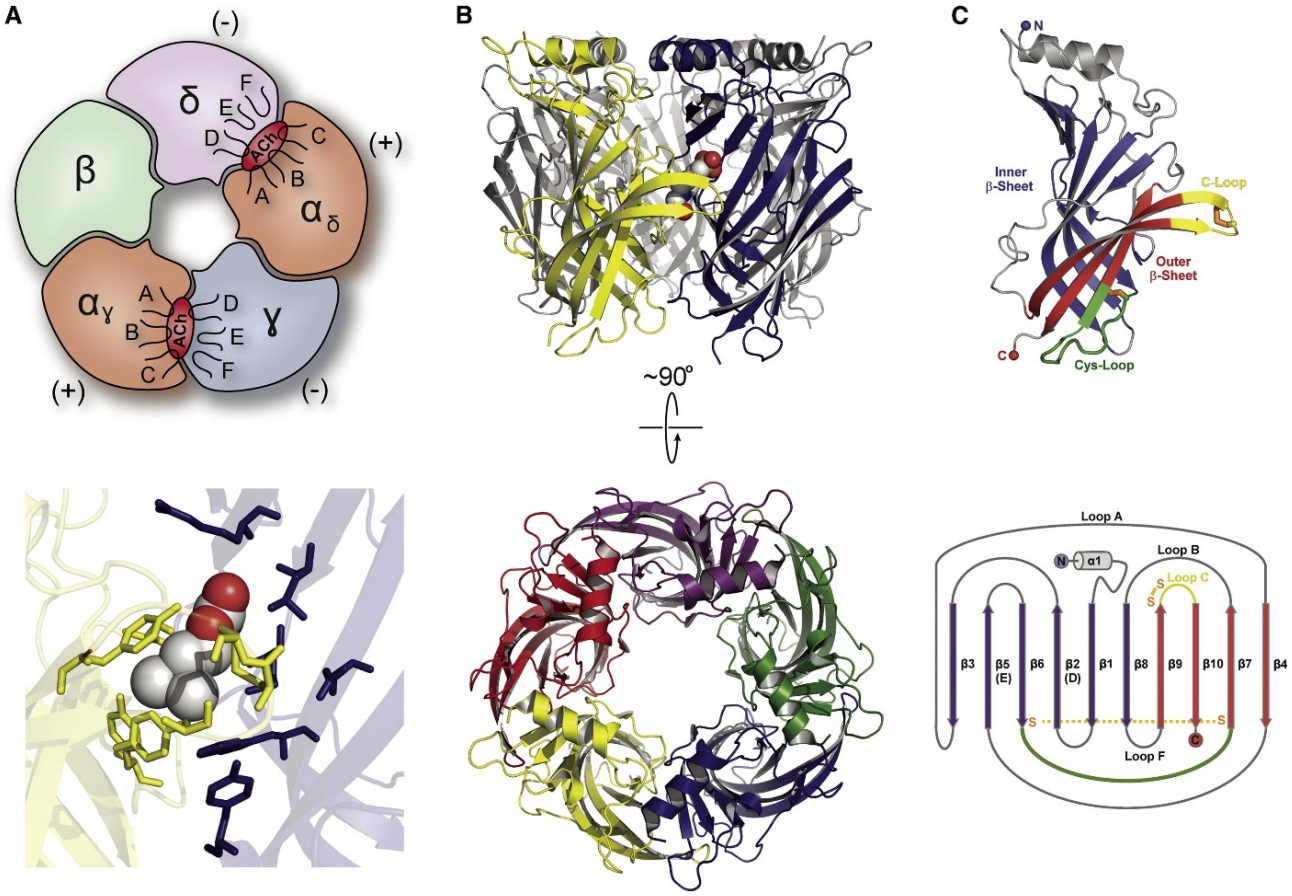


**Figure 1.2 The extracellular domain structure.**

(A) The top image is a top-down cartoon representation of the *Torpedo* nAChR ECD. Acetylcholine molecules are depicted in red at the interface of the principal α (+) and complementary δ, γ (-) subunits, with loops A, B, C and D, E, F overlapping with the molecule in their respective subunits. The bottom image is a close-up side view of the *Lymnaea stagnalis* AChBP bound to carbamylcholine (PDB: 1UV6). The principal and complementary face is highlighted in yellow and blue, with interacting residues depicted as sticks and backbone polypeptide shown as a transparent cartoon. Carbamylcholine is highlighted as multicoloured spheres. (B) Side and top view of AChBP (PDB: 1I9B) tertiary structure with coloured subunits and a bound HEPES molecule shown as multicoloured spheres. (C) A single AChBP subunit's tertiary fold represented as a cartoon from a side-view. The N-terminal α-helix, inner β-sheet (β1, β2, β3, β5, β6 and β8 strands) and outer β-sheet (β4, β7, β9 and β10) are highlighted in gray, blue and red respectively. The bottom image is a topology map of AChBP with the same colouring scheme highlighting the location of the Cys-loop (green), C-loop (yellow) and A, B, D, E, F loops. Figure was reprinted from Structure, 21, daCosta, C. J. B., and Baenziger, J. E., Gating of pentameric ligand-gated ion channels: Structural insights and ambiguities, 1271-1283., 2013, with permission from Elsevier.

## 1.5 The TMD and Ion Permeation

The TMD within each subunit is made up of 4 α-helices (M1-M4) that arrange in a helical bundle. M2 helices line the channel pore and interact with the M1-M3 helices, which shield the M2 and channel pore from the lipid environment of the plasma membrane. The outermost helix is M4, which forms the receptor-membrane interface.

Ions flow down their electrochemical gradient, passing through a wide vestibule in the ECD (Hansen et al., 2008). A negative electrostatic surface potential of the ECD is responsible for funneling cations into the M2 α-helices that line the channel gate (Imoto et al., 1988; Rahman et al., 2020). Prior to entering the M2 gate, a ring of charged or polar residues at the 20' position is responsible for ion selectivity and channel conduction (Imoto et al., 1988). In α1 and α7 subunits, this 20' residue is a glutamate, whilst in ELIC, it is an asparagine (Figure 1.3B). Three rings of hydrophobic residues follow at positions 16', 13', and 9' which correspond to phenylalanine, alanine, and leucine in ELIC. In the α1/α7 nAChR subunits, these three rings correspond to leucine, valine, and leucine. The narrowest constriction of the pore is formed by these hydrophobic rings in the closed conformation of the channel. Specifically, in the muscle-type receptor, a 2.8 Å and 2.9 Å pore constriction is present at the level of the 9' and 16' hydrophobic residues, respectively (Rahman et al., 2020). This narrow constriction serves as an energetic barrier for hydrated ion permeation, where a hydrated sodium or potassium is around 8 Å in size, forming a hydrophobic gate (Miyazawa et al., 2003; Beckstein and Sansom, 2006; Ivanov et al., 2007). Binding of an agonist leads to the movement of M2 α-helices to effectively widen the channel pore, by breaking the Van der Waals interactions that stabilize these constrictions. Once ions emerge from the channel gate, they are exposed to two polar rings

at the 6’ and 2’ positions, which are most frequently either a serine or threonine in nAChRs, or a threonine and glutamine in ELIC (Figure 1.3B). To enter the cytoplasm of a cell, the last structure through which the ions must transport through are lateral portals in the CD of nAChRs (Miyazawa et al., 1999). Presented with five conduction pathways, cations pass through lateral portals, which are formed by the MX α-helix, post M3-loop, and MA α helices (Kelley et al., 2003). The -1’ glutamate portal residue serves as the final determinant of cation selectivity and conductance (Corringer et al., 1999; Gunthorpe and Lummis, 2001). In ELIC, due to the absence of a CD, cations adopt a single conduction pathway that is also lined at the -1’ position with a glutamate residue.

For ions to permeate the receptor, an agonist needs to bind in the ECD, and this binding must be linked to the M2 α-helices of the TMD. A region that is crucial for efficient communication between these two domains is the extracellular-transmembrane domain interface.

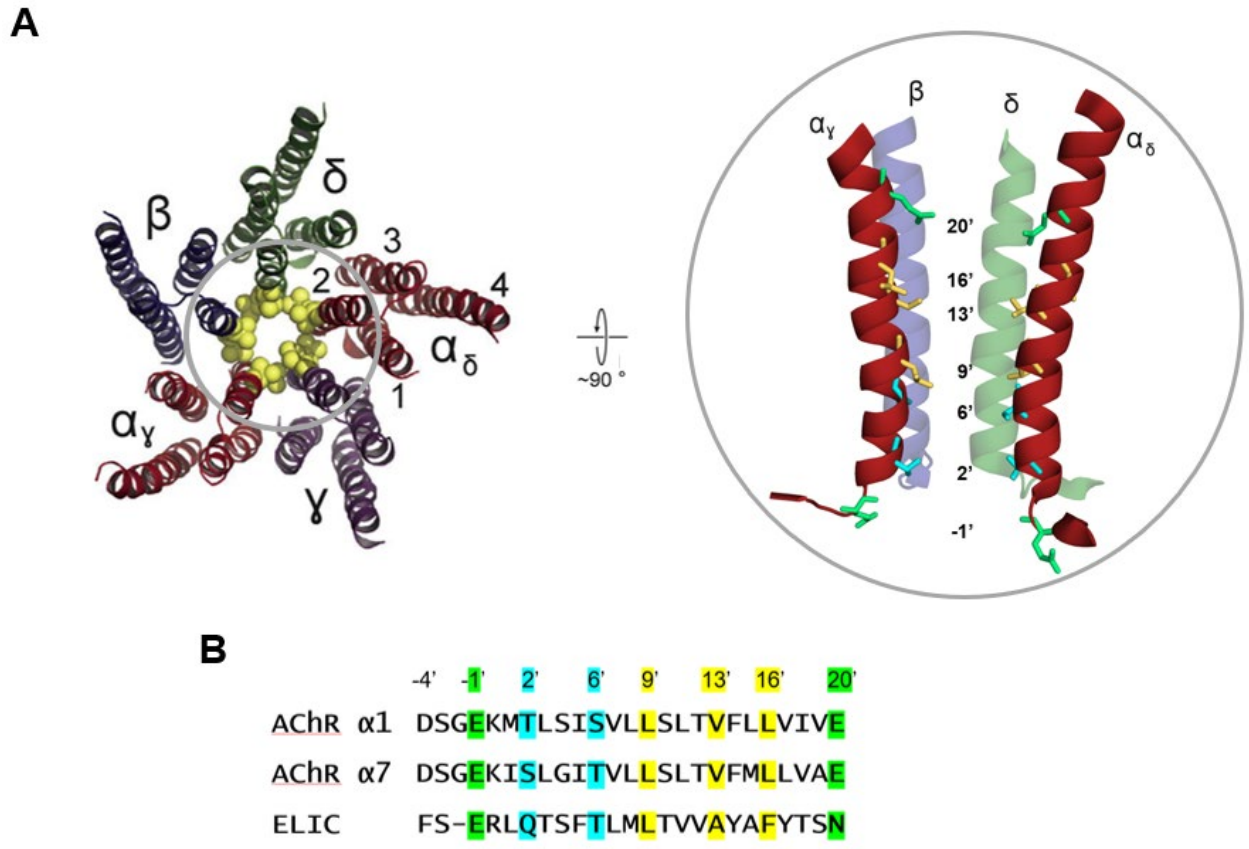


**Figure 1.3 The transmembrane domain structure and ion permeation pathway of a pLGIC.**

(A) On the left is a top-down cryo-EM structure of the *Torpedo* nAChR (PDB: 2BG9) TMD. The different subunits (α, red; β, blue; γ, purple; δ, green) are highlighted and the $\alpha_\delta$ subunit is annotated, indicating the position of helices M1-M4 in the four-helix bundle. The side chains of residues forming the channel gate (αL251 and αV255 and analogous β-, γ- and δ-subunit residues) are represented as yellow spheres. On the right is a side profile of the $\alpha_\delta$, $\alpha_\gamma$, β and δ M2 helices, which line the channel pore (γ is excluded to illustrate the side chain residues). Residues in the $\alpha_\delta$ and $\alpha_\gamma$ M2 helices that line the channel pore are shown as sticks with their position in the prime (') notation. (B) M2 helix sequence alignment of $\alpha_1$, $\alpha_7$ and ELIC receptor subunits, with prime numbering indicated above for key regions. Hydrophobic residues that form the channel gate, hydrophilic residues that interact with the ion, and charged/polar residues that are key to cation selectivity are highlighted in yellow, cyan, and green respectively. The left panel A figure was reprinted from Structure, 21, daCosta, C. J. B., and Baenziger, J. E., Gating of pentameric ligand-gated ion channels: Structural insights and ambiguities, 1271-1283., 2013, with permission from Elsevier.

## 1.6 The ECD-TMD Coupling Interface

The site of agonist binding is found roughly 50 Å away from the channel gate. Structural changes need to propagate across this distance through critical regions of the receptor. The best-established region to relay this signal is the extracellular-transmembrane domain interface. From the ECD, this network is composed of loops β1-β2, β6-β7 (also known as the cys-loop), and β8-β9 (Figure 1.4). The TMD contributes the pre-M1 linker, M2-M3 linker and the C-terminal end of M4 (Figure 1.4). Interaction between the ECD loops with the pre-M1 linker and M2-M3 linker have been shown for both ELIC and the nAChR (Unwin et al., 2002; Miyazawa et al., 2003; Hilf and Dutzler 2008; Lee et al., 2008). The AChBP contains the three key ECD loops; however, it lacks a TMD interface for interaction that would relay the signal of agonist binding to channel gating.

Chimaeric studies that combine the AChBP with the pore domain of a 5-$HT_3$A receptor were able to express channels that bind ACh, but are not activated for ion conduction (Brejc et al., 2001; Bouzat et al., 2004). By changing the β1β2, cys-loop and β8β9 loops in AChBP to $5HT_3$A residues, this chimaera was rendered functional (Bouzat et al., 2004). Thus, compatibility between these interface loops is key to transmitting the signal from agonist binding to channel gating. This study highlighted that the AChBP can undergo conformational changes upon ACh binding that, in a pLGIC, would lead to the opening of the channel gate.

A principal allosteric pathway linking agonist binding to channel gating in a muscle-type nAChR α subunit involves key residues in these interface loops (Lee and Sine, 2005). The pathway begins with a C-loop capping motion over the bound agonist, where rigid-body movements of β10 containing a key R209 residue result in its extension into the hydrophobic

core of the subunit. Subsequently, E45 located on the β1-β2 loop electrostatically interacts with this arginine, causing the neighboring V46 to straddle P272 located in the M2-M3 linker, and to fit inside a cavity created by S269 and P272 in the M2-M3 linker. Structural changes in the M2-M3 linker then propagate to the M2 α-helix lining the channel pore. The key salt bridge in this pathway has been verified by high-resolution structures of the α-subunit ECD (Dellisanti et al., 2007) and GLIC (Hilf and Dutzler, 2008). Moreover, equivalent salt bridge interactions are present in the $GABA_A$ and $GABA_C$ receptors (Wang et al., 2007).

Specific residues in the ECD-TMD coupling interface that are responsible for linking agonist binding to channel gating have not been identified in ELIC. However, the importance of compatibility between these interface loops for agonism has been shown in the ELIC ECD - α7 nAChR TMD chimaera (Tillman et al., 2014). This chimaera is not activated by the native ELIC agonist cysteamine, due to incompatibility with the α7 nAChR. In the α7 nAChR, the C-terminus and M2-M3 linker are longer, and differ in amino acid composition, compared to ELIC. By truncating and substituting these regions with the shorter ELIC C-terminus and M2-M3 linker, a functional chimaera was produced (Tillman et al., 2014).

Another chimaeric study involving an α7 nAChR ECD - $5HT_3A$ TMD receptor, which compared the kinetics of activation and desensitization, provided further insight into the importance of these interface loops (Bouzat et al., 2008). The α7 nAChR receptor desensitizes rapidly with isolated brief opening events during channel activation, unlike $5HT_3A$, which has a slow decay rate and long openings. The chimaera, unlike the parent receptors, has a distinct intermediary open duration and an overall intermediate kinetic profile, between the parents. Reconstructing the loops in this chimaera at the interface of the two domains to completely resemble the $5HT_3A$ residues, or to completely resemble the α7 residues, had the result of

recapitulating the parent kinetic profiles. These studies highlight the importance of the ECD-TMD interface loops in relaying structural information from agonist binding to channel gating. One question that emerges is whether binding of an agonist is a prerequisite for channel activation. Another concerns the other conformations these receptors transition through when bound by an agonist.

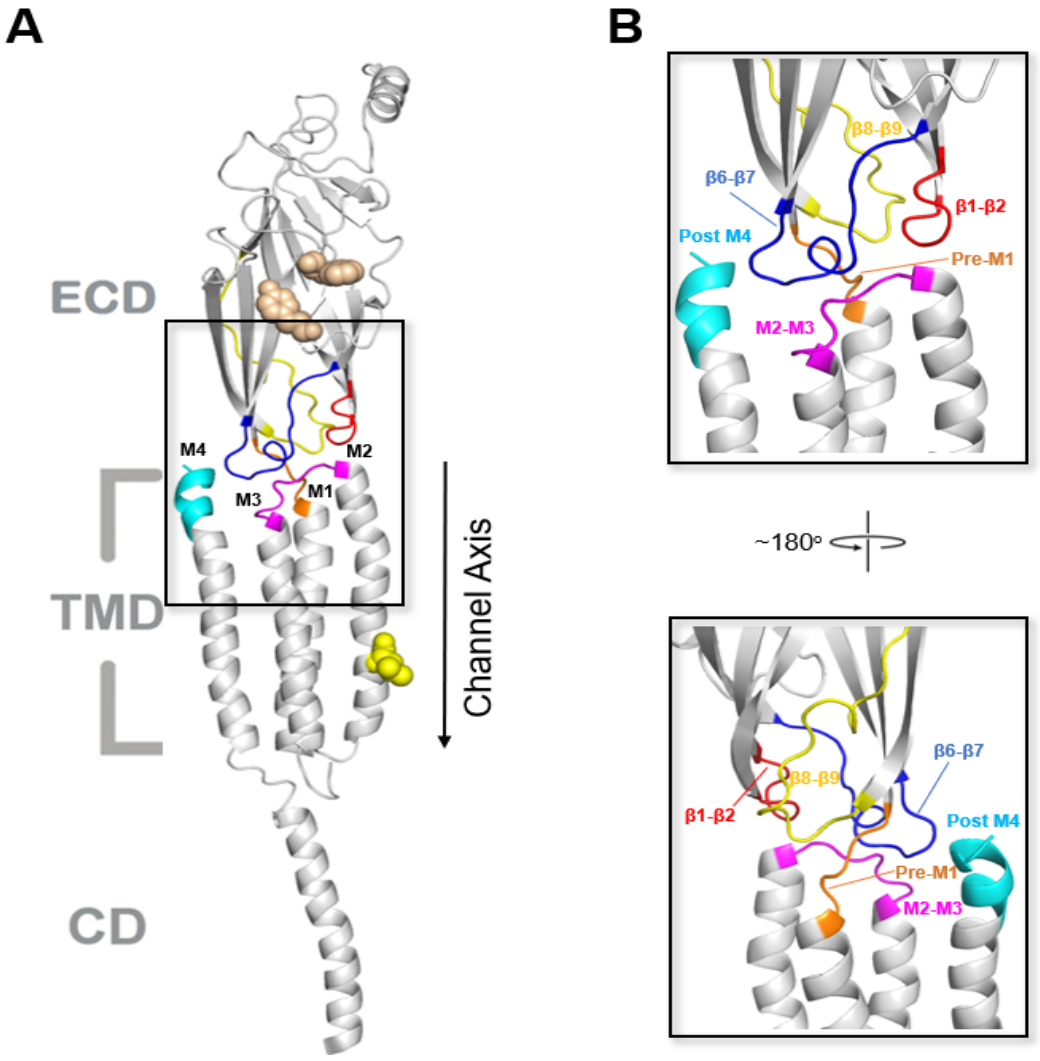


**Figure 1.4 The extracellular–transmembrane domain interface.**

The above images are a cartoon representation of the $\alpha_1$ *Torpedo* nAChR subunit (PDB: 2BG9). (A) View from the plane of the membrane depicting the ECD, TMD and CD domains with the channel axis and M1-M4 α helices annotated. Orthosteric site residues W149, Y93 and the channel gate residue L251 are shown as tan and yellow spheres, respectively. The coupling interface structures (solid box) are highlighted, and include the C terminal end of M4 (post-M4) in cyan, β6-β7 loop (Cys-loop) in blue, M2-M3 linker in magenta, pre-M1 in orange, β8-β9 loop in yellow and β1-β2 loop in red. (B) Close-up view of the coupling interface structures from the front and back, which are annotated with the same colouring scheme as in A.

## 1.7 Channel Activation and Conformations

Receptors in the pLGIC superfamily transition between at least three structurally and functionally distinct conformational states (Figure 1.5). Each conformation contains different affinities for the agonist, with only the open state allowing ion conduction. One of these conformations is the resting state, in which the channel pore is closed, occluding the passage of ions, with no agonist bound. Agonist binding results in a transition to a second conformation, the active state, in which the channel is open and allows ion passage. Prolonged exposure to agonist leads to a third conformation, the desensitized state. The desensitized state is characterized by the presence of agonists bound to the channel, with a structure of the pore that obstructs ion passage. A fourth non-functional conformation, termed the uncoupled conformation, has also been documented in the nAChR (daCosta and Baenziger, 2009). This occurs in the absence of anionic lipids and cholesterol, when the nAChR binds an agonist but does not undergo agonist-induced conformational transitions.

To describe how an agonist leads to channel activation, the induced-fit model was initially proposed. In the induced-fit model, substrate binding is the driving force and a prerequisite for conformational change (Koshland 1959). Another famous model proposed to describe allosteric enzyme activity is the Monod-Wyman-Changeux (MWC) theory. The MWC theory states that pLGICs can spontaneously switch between pre-existing states and that ligands shift the equilibrium to the states for which they display the highest binding affinity (Monod et al., 1965). Another aspect of the MWC theory is the conserved symmetry among the different populated states of the receptor. In the simplest form, two symmetrical states, a low affinity resting state and high affinity active state, are in equilibrium. Subsequent ligand binding

incrementally shifts this equilibrium towards the active state. This model provides an explanation of the cooperativity involved with ligand binding and the mechanism by which ligands activate a channel. Support for the MWC model of pLGIC activity comes from the fact that the nAChR opens infrequently and for brief durations in the absence of agonist (Jackson 1984). These spontaneous unliganded transitions have been identified for gain of function mutations and extrapolated to the WT nAChR channel, indicating that the channel opens for approximately 80 μs once every 15 min (Purohit and Auerbach, 2009).

Evidence from electrophysiology experiments identified that activation does not simply follow a two-step model of resting/closed and active/open, but instead follows many steps with short-lived intermediary conformational states. The first instance of an intermediate state was described as "flipped", which was identified in the alpha-1-beta glycine receptor and muscle-type nAChR (Burzomato et al., 2004; Lape et al., 2008; Sivilotti, 2010). This "flipped" F state is characterized by a high-affinity conformation of the orthosteric site, with a closed channel. Agonist efficacy determines the rate of entry into the "flipped" state, but subsequent channel opening is independent of agonist efficacy (Lape et al., 2008). Evidence of two distinct transient closed, or "primed", states was identified for the muscle-type nAChR; these give rise to two distinct channel opening states (Mukhtasimova et al., 2009). The singly primed state is intermediate in duration and produces short channel opening, whilst the doubly primed state is short in duration and produces long channel opening. Not only are there multiple conformational states responsible for activation, pLGICs adopt two structurally and functionally separate desensitized states (Heidmann and Changeux, 1980; Sakmann et al., 1980; Yamodo et al., 2010; Keramidas and Lynch, 2013). Desensitization is the highest affinity state for the agonist, where a fast-desensitized conformation is followed by a slow long-lived desensitized conformation. As a

result, the MWC model was extended to account for the desensitized states, to portray the channel as converting from resting, to active, to fast desensitized and long desensitized states (Heidmann and Changeux, 1978; Edelstein et al., 1996). Improved statistical fit for kinetic models incorporating intermediate states of muscle-type nAChR and other pLGICs further supports the presence of these states in other channels (Krashia et al., 2011; Marabelli et al., 2015).

Out of the vast number of molecules in the extracellular space, only a select few can bind pLGICs, and of these, only a subset are able to activate them.

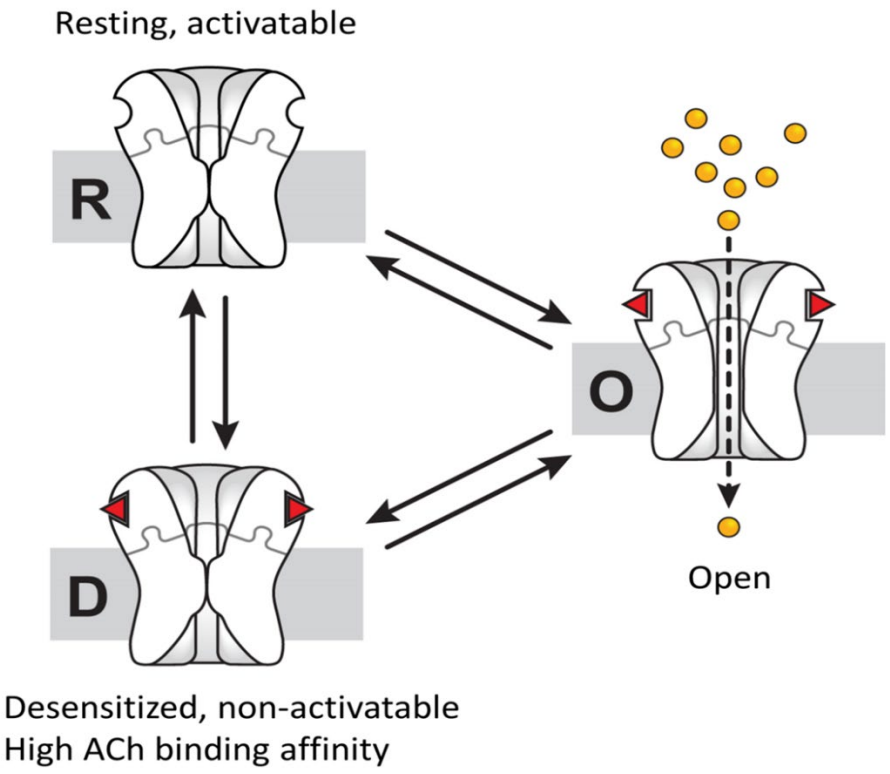


**Figure 1.5 pLGIC conformations.**

(A) Illustration of the muscle-type nAChR starting from the resting state (R), where transitions to desensitized (D) or open conformation (O) can occur. Channels can also transition to the desensitized state from the open conformation. Agonist (red triangle) binding to the ECD is shown in the desensitized and open conformations. Ion passage (orange circles) is depicted in the channel open conformation. Figure was reprinted from Structure, 21, daCosta, C. J. B., and Baenziger, J. E., Gating of pentameric ligand-gated ion channels: Structural insights and ambiguities, 1271-1283., 2013, with permission from Elsevier.

## 1.8 Agonists and Competitive Antagonists

An agonist and competitive antagonist bind to the same binding site. Competitive antagonists exert an inhibitory effect on channel function by effectively blocking agonist binding to the orthosteric site, and they themselves cannot induce channel opening. Large competitive antagonists, such as the 8 kDa polypeptide α-bungarotoxin, sterically occlude agonist binding and stabilize an open C loop conformation (Rahman et al., 2020). The muscle-type and α7-α10 containing nAChRs are inhibited by α-bungarotoxin (Rahman et al., 2020). In contrast, the binding of an agonist can activate the channel to conduct ions. The binding pocket residues of ELIC most closely resemble the $GABA_A$ receptor, and the agonist GABA of this inhibitory channel can also activate ELIC (Miller and Smart, 2010; Zimmermann et al., 2011; Spurny et al., 2012). Generally, ELIC is activated by small unbranched primary amines including alkylamines, aminothiols (e.g. cysteamine), aminoalcohols, bromoamines, diamines and GABA; the exceptions to these are the partial agonists Gamma-hydroxybutyric acid (GBH) and 5-aminovaleric acid (5-AV) (Zimmermann and Dutzler, 2011; Thompson et al., 2012). The nAChRs are generally activated by molecules that contain a quaternary amine group. The defining agonist of the nAChR family is ACh, with AChBPs showing the same ligand specificity (Smit et al., 2001). Whilst ELIC is not activated by nAChR agonists, ACh is capable of binding to the orthosteric site, with comparable affinity to the ELIC agonist GABA (Pan et al., 2012). ACh is a competitive inhibitor of ELIC that reversibly binds to the orthosteric site and triggers loop C closure, but these structural changes do not lead to cation conduction (Pan et al., 2012).

## 1.9 ELIC is Competitively Inhibited by ACh

ACh acts as a competitive antagonist of ELIC (Pan et al., 2012). The quaternary amine group of ACh is positioned inside an aromatic cage formed by residues in loop B (F133), loop C (Y175 and F188), loop D (Y38) and loop G (F19), a feature found in nAChRs (Brejc et al., 2001; Unwin, 2005; Li et al., 2011). This quaternary amine group interacts with loop B E131 and loop A E77 electrostatically (Figure 1.6B). Residues F133, Y175 and F188 form cation-π interactions with the quaternary amine as well. On the complementary face, the acetyl group of ACh hydrophobically contacts Y38 and F19. These binding site contacts stabilize a conformation of ELIC, by causing the tip of loop C to shift by ~6 Å and close over the ligand with reduced flexibility (Pan et al., 2012). Additionally, a concerted counter-clockwise rotation of loops B and C in the upper part of the ECD, and a clockwise rotation of the lower region ECD loop F and β10 occurs. These structural changes resemble the AChBP and α7 nAChR–AChBP chimaera upon agonist binding (Hansen et al., 2005; Celie et al., 2005; Li et al., 2011). The coupling interface residues in the β1–β2 loop and the M2-M3 linker are almost unchanged upon ACh binding. Only the β6-β7 loop undergoes structural changes, by reorienting its side chain residues. Structural changes propagate to the channel gate M2 F247 residues, which rotate slightly away from the central pore, producing an enlargement of ~1.32 Å in this region (Pan et al., 2012). This widening of the pore is not enough to conduct ions. To determine this, two-electrode voltage clamp (TEVC) experiments were conducted, in which acetylcholine reversibly inhibited cysteamine currents in a concentration-dependent manner (Pan et al., 2012).

The difference between an agonist and competitive antagonist is subtle. The authors were able to create agonism in ELIC from an ACh derivative, 2-methylaminoethylacetate (DMAEA)

(Pan et al., 2012). To produce DMAEA, a single hydrogen atom was substituted in the place of a methyl on the quaternary amine group of ACh (Pan et al., 2012). This substitution exposes the cationic nitrogen atom to form stronger interactions with the acidic and aromatic residues in the principal subunit. In the glycine and GABA receptors, the opposite strategy was utilized; methylation was used to convert a primary amine agonist into an antagonist, by shielding the cationic nitrogen (Breckenridge et al., 1981; Schmieden and Betz, 1995). The authors suggested a few residues that differ between nAChRs and ELIC; the thought was that these may be responsible for the inability of ACh to activate the channel. Residue I79 is a tyrosine in the nAChR family, with its side chain hydroxyl group hydrogen bonding with ligands in AChBPs (Hansen et al., 2005; Figure 1.6C). The residue F133 is a tryptophan that is closer by 1.2 Å to the quaternary amine of ACh, forming strong cation-π interactions in AChBPs (Brams et al., 2011; Figure 1.6C). While not all agonists interact with the same residues in the binding site to activate a receptor (Thompson et al., 2010), it is interesting to note that GABA and ACh adopt practically the same binding pose in ELIC (Figure 1.6B). Additionally, the quaternary amine of ACh in the agonist-binding site is positioned in a similar orientation in AChBPs (Pan et al., 2012; Olsen et al., 2014; Figure 1.6C).

Given that the ACh derivative DMAEA activates ELIC, further exposure of the cationic nitrogen in primary amines such as GABA highlights that the interactions made with this nitrogen may be significant for agonism. The two suggested binding site mutations, I79Y and F133W, may lead to stronger interactions with the quaternary amine of ACh to promote ELIC agonism. Agonism consists of key amino acid residues that are in direct contact with the ligand, as well as those that link agonist binding to channel gating. Identifying residues that are coupled along the allosteric pathway would be extremely valuable for ensuring that binding with higher

affinity also leads to channel activation. These coupled residues would serve as sites that can be mutated in isolation or simultaneously to improve the communication between the two regions in the presence of ACh. In order to identify a group of coupled residues responsible for ACh agonism, statistical coupling analysis (SCA) was performed.

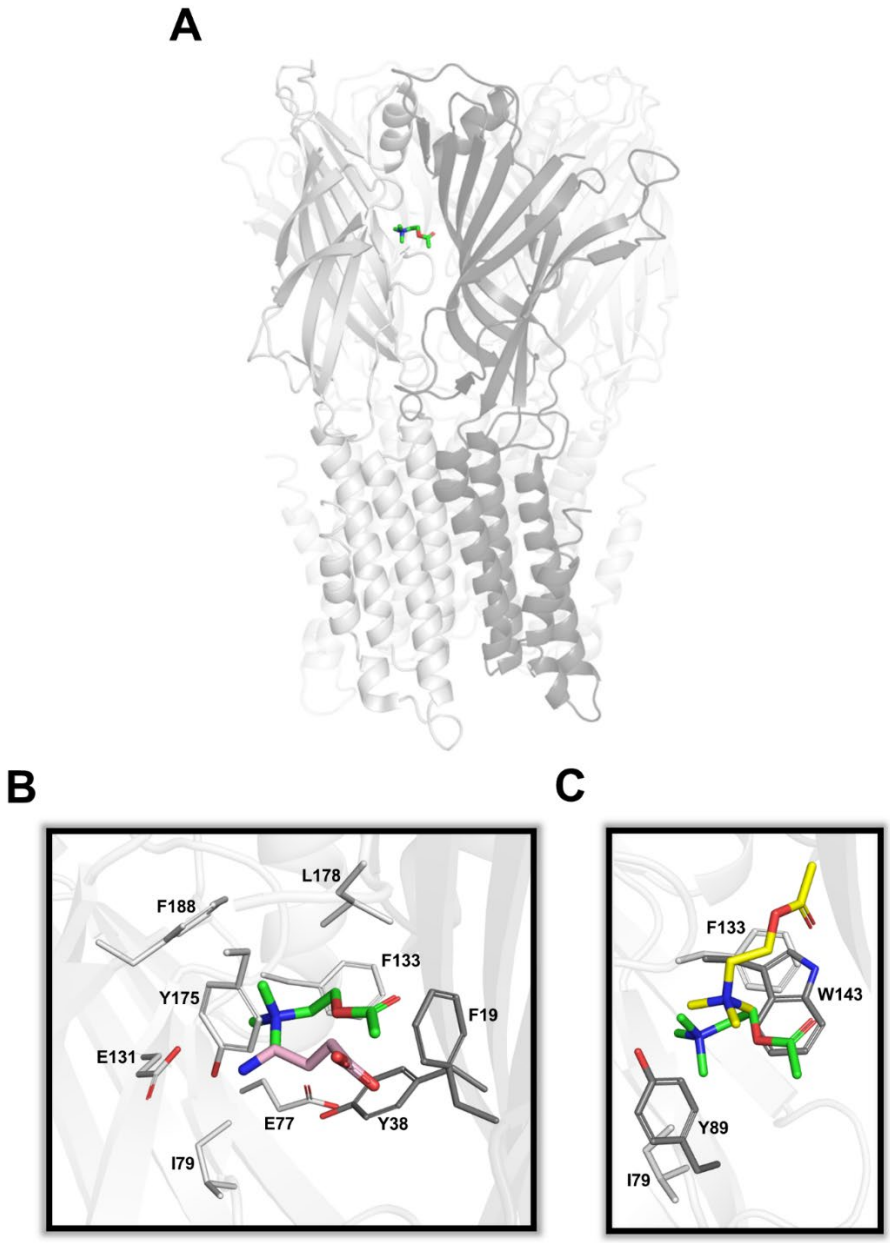


**Figure 1.6 Orthosteric site binding pose of ACh along with GABA in ELIC and ACh in AChBP. (**A) ELIC crystallized with ACh (PDB: 3RQW) is shown as a cartoon representation with the principal subunit coloured in light gray and complementary subunit in dark gray. (B) Close-up of the agonist binding site is shown. Binding pocket residues F19, Y38 on the complementary face (carbon = dark gray, oxygen = red) and E77, I79, E131, F133, Y175, L178, F188 on the principal face (carbon = light gray, oxygen = red) are highlighted as sticks. The align algorithm was used in PyMOL to align GABA from the ELIC crystal structure (PDB: 2YOE) to ELIC crystallized with ACh (PDB: 3RQW) with a Cα RMSD of 0.43 Å. Both ACh and GABA are shown as sticks, where carbon atoms are highlighted in green and pink respectively, with nitrogen in blue and oxygen in red. The C-loop has been removed for clarity. (C) The CE align algorithm was used in PyMOL to align ACh and residues Y89, W143 from the AChBP crystal structure (PDB: 3WIP) to the ELIC ECD (PDB: 3RQW) with a Cα RMSD of 3.5 Å. In the AChBP ACh is represented as a stick with carbons coloured in yellow, nitrogen in blue and oxygen in red, whilst ACh in ELIC is represented as in (B). Residues I79 and F133 in ELIC (carbon = light gray) along with homologous position Y89 and W143 in AChBP (carbon = dark gray, oxygen = red, nitrogen = blue) are shown as sticks.

## 1.10 Statistical Coupling Analysis

Evolution provides a wealth of mutagenesis data that has been acquired over million/billions of years in a protein family. Identifying the global pattern of physical interactions between amino acids in a folded protein structure is a challenging task. Traditionally, local physical interactions between residues in a protein would be determined using thermodynamic mutant cycle analysis (Carter et al., 1984; Fersht et al., 1992; Hidalgo and Mackinnon, 1995). In this method, two single mutants and the corresponding double mutant's binding energy is determined. The two residues can be deemed not to energetically interact if the change in free energy of the double mutant is the sum of the two single mutants; this would indicate that the effect of each mutation is independent (Figure 1.7A). Otherwise, if the change in free energy of the double mutant is not additive, the two residues must be coupled. Using this technique to map all the energetic interaction in a protein is impractical, requiring thousands of mutations to be fully characterized.

To simplify this problem, a method termed statistical coupling analysis (SCA) was developed that utilizes the evolutionary sequence data of a protein family (Lockless and Ranganathan, 1999). First, a large and diverse ensemble of protein family sequences, which share the same or similar function, are all aligned to ensure that homologous positions between all the proteins are in the same column. Using this alignment, the conservation of an amino acid at position *i*, which is the measure of evolutionary constraint of an amino acid at that position, is determined for all of the protein sequence positions (Figure 1.7B). This conservation value is calculated by comparing the frequency of a particular amino acid at position *i* to the random expectation, which is the mean abundance of that amino acid in all proteins. These evolutionary

constraints at different positions may not be independent, meaning that positions *i* and *j* may interact with each other and undergo pairwise coevolution. In the case of coevolution, the composition at *j* controls or exerts a natural selective pressure on the amino acid composition at *i* (Figure 1.7B). The degree to which amino acid frequencies at all sites, *i*, change in response to a change in *j*, is then calculated, to produce a full-scale mapping of statistically coupled sites or a correlated group relative to position *j*.

A diagonally symmetric statistical coupling matrix emerges by plotting the degree of coevolution at all positions, *i*, against all sites, *j*, in a protein (Figure 1.7C). To determine the global pattern of functional correlations between amino acids in a protein, the matrix needs to be adjusted (Halabi et al., 2009). Due to limited sampling of sequences, some of the correlated groups in this matrix are the result of statistical noise. To determine the significant correlated groups, a random correlation matrix is created by scrambling the columns in an alignment independently for many iterations. The degree of coevolution between positions in this random alignment is then calculated. From the comparison of this random correlation matrix to the actual one, the functionally significant correlations can be deduced. All the statistically non-random information in the matrix is decomposed into groups of coevolving amino acids, called protein sectors (Halabi et al., 2009). The protein sectors identified in the S1A serine protease, WW, PDZ, PAS, SH2 and SH3 protein families, are physically contiguous in the tertiary structure and contribute to a distinct functional role in the protein (Hatley et al., 2003; Shulman et al., 2004; Russ et al., 2005; Ferguson et al., 2007; Halavaty and Moffat, 2007; Lee et al., 2008; Halabi et al., 2009; Smock and Gierasch, 2009).

These coevolving amino acids in a sector reflect how two or more sites in a protein functionally communicate. Mutagenesis studies have previously implicated residues within

sectors as being key for phenotypic traits of a protein such as binding affinity, denaturation temperature and allosteric behaviour (Hatley et al., 2003; Halavaty and Moffat, 2007; Halabi et al., 2009; Smock and Gierasch, 2009). Alteration of the agonist specificity of a protein is achieved by altering residues within these sectors, rather than by altering non-sector residues. Only two sector mutations at distant locations in the PSD95 PDZ domain can alter the specificity towards a class-switching ligand (McLaughlin et al., 2012). A sector responsible for ACh agonism is likely present in the nAChRs and AChBP. Prior to performing SCA, a multiple sequence alignment (MSA) of several hundred members needs to be conducted with proteins that share folding and function (Russ et al., 2005, Halabi et al., McLaughlin et al., 2012). To do this, the *Lymnaea stagnalis* AChBP was used as a representative protein because its high-resolution crystal structure (2.6 Å) is available with ACh bound to the agonist binding site (Olsen et al., 2014). By using the sequence and structural information from this AChBP-ACh crystal structure, we were able to obtain thousands of sequences that resemble the 3D structure of ACh bound to AChBP.

In the present thesis, the AChBP was used as a model system for identifying the positions responsible for ACh agonism. In the case that the amino acid composition between an AChBP sector responsible for ACh agonism differs from ELIC at homologous positions, then these differing residues would serve as sites that can be mutated to their AChBP identity. By recreating either parts of, or the entire protein sector from AChBP in ELIC, an optimized system of binding ACh could be achieved; this may allow for channel gating.

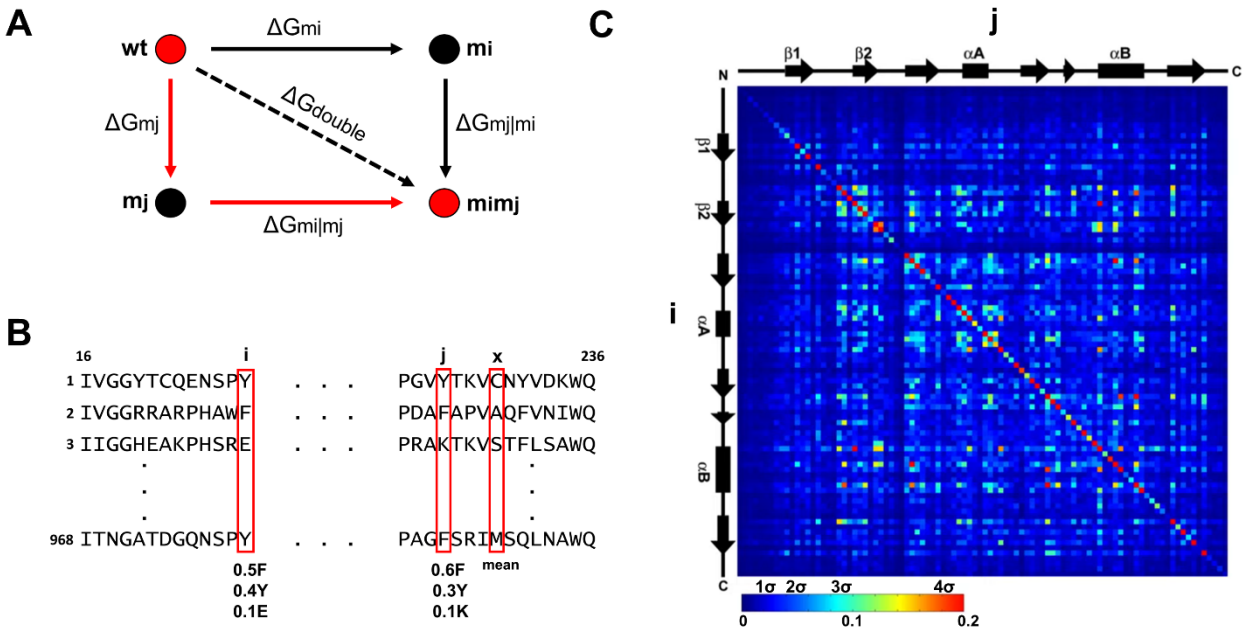


**Figure 1.7 Statistical coupling analysis.**

(A) Thermodynamic mutant cycle analysis for a double mutant. A mutation (m) at positions *i* and *j* are independent if the sum of the Gibbs free energy change of each mutation (ΔGmj and ΔGmi) is equal to the Gibbs free energy change of the double mutant (ΔGdouble). (B) Multiple sequence alignment between 968 members of a protein family with the longest sequence being 236 amino acids. Positions *i*, *j* and *x* are highlighted in red where the conservation values of the most frequent amino acids at these positions are written below. The amino acid composition of position x approaches the mean value in all proteins, thus it equal to the random expectation. (C) The SCA correlation matrix for an alignment of 240 PDZ domains. Secondary structure elements are shown on each axis for the 92 amino acid long sequence, where the horizontal axis is labelled as position *j* and vertical axis as position *i*. Correlation strength is depicted below in the colour scheme where blue indicates weak correlations and red a strong correlation. The panel C figure was reprinted from Cell, 138, Halabi, N., Rivoire, O., Leibler, S., and Ranganathan, R., Protein Sectors: Evolutionary Units of Three-Dimensional Structure, 774-786., 2009, with permission from Elsevier

## 1.11 Thesis Objectives

The goal of this thesis is to transform the competitive antagonist, ACh, into an agonist for ELIC, using mutations guided by statistically coupled positions in AChBP. To do so, SCA was performed on the MSA of AChBPs; three protein sectors emerged. The composition of residues in the sector from AChBP that presented more positions at its orthosteric site was compared to homologous positions in ELIC. A total of 15 positions differed in residue composition between the AChBP sector and ELIC; of which, we only focused on four. The four positions were selected based on the proximity of the residue to bound ACh in the ACh-ELIC complex structure. These positions were also selected because the corresponding AChBP residues, which are conserved in AChRs, have been previously implicated in ACh agonism. Each single mutant was created using site-directed mutagenesis, whilst the double, triple, and quadruple mutants were ordered from Twist Bioscience. The mutants were subsequently analyzed using two-electrode voltage clamp (TEVC) electrophysiology for expression and response to the native agonist, cysteamine, as well as to ACh.

First, we identify that WT-ELIC residues are optimized for cysteamine agonism, as most of the mutants decrease the potency of this native agonist. Then, we show that none of the mutants are activated by ACh, but that the potency with which ACh inhibits the receptors is decreased for two key single mutants. By combining these two mutations, we effectively knock out ACh inhibition. To explore further the effect of ACh on this double mutant, a range of cysteamine concentrations are used with and without ACh present. From this, we identify that ACh is a potentiator of cysteamine-induced currents in the double mutant. This study highlights the utility of SCA as a method to identify functionally important residues in pLGICs, and that

ACh can be converted from a competitive inhibitor to a potentiator of ELIC, with the substitution of only two AChR residues.

# Chapter 2 - Experimental Procedures

## 2.1 Homologous Sequence Search and Multiple Sequence Alignment

The *Lymnaea stagnalis* AChBP PDB structure 3WIP was used to search for homologous protein sequences following the Rosetta-Hmmer (Rd.HMM) protocol (Martinez-Castilla and Rodriguez-Sotres, 2010; Appendix Figure 4.3A). First, Rosetta 3.9 software suite was used to design proteins of the same length and 3D structure as the first subunit of the 3WIP PDB file (Chain A), as AChBP is a homomer. As all of the Rosetta-designed sequences are the same length, and as the residue at each position is derived from the WT residue, they can be considered directly aligned to the original WT sequence. These trivially aligned sequences were used to build a profile hidden Markov model or profile HMM with the *hmmbuild* tool from the HMMER 3.2.1 suite. Finally, the UniRef100 protein sequence database was queried with the profile HMM by using the *hmmsearch* tool; this yielded 7132 sequences with an E-value less than or equal to 0.01.

A multiple sequence alignment (MSA) was then created with the *hmmalign* tool with the corresponding homologous 7132 sequences. Sequence pairs that exceeded a 90% cutoff amino acid identity were removed using the CD-HIT tool. The final yield was 1438 sequences; this included the original 3WIP subunit sequence.

The homologous sequence search and MSA described above, in addition to the SCA, were performed by Dr. Jesús Agustín Banda-Vázquez.

## 2.2 Statistical Coupling Analysis

The SCA v5.0 toolbox (McLaughlin et al., 2012) was used to analyze the multiple sequence alignment generated from the AChBP 3WIP subunit. A gap cut-off of 0.4 was used, meaning that the alignment was truncated to sequence positions with a gap frequency of less than 40%. A kmax value of 4 was chosen, which corresponds to the top number of eigenmodes that are transformed into k maximally independent components. The first three independent components are the basis of three sectors where a cut-off of 0.95 was used to define the positions included in a sector, having a statistically significant position correlated weight.

The corresponding sector residue positions from AChBP (PDB: 3WIP) were mapped to ELIC (PDB: 3RQW), and any residues that appeared as gaps were resolved by using the super algorithm in PyMOL to structurally align their Cα atoms, with a RMSD of 3.5 Å.

## 2.3 Molecular Biology

The WT ELIC-pTLN plasmid was kindly provided by Dr. Raimund Dutzler (Zimmermann et al., 2012). A C-terminal alanine, a cloning artifact not present in the GenBank sequence (GenBank: POC7B7), was removed. The ELIC plasmid has the α7 nAChR signal sequence followed by the ELIC coding sequence (Appendix Figure 4.3B). Inverse PCR was used to create the point mutants (Silva et al., 2017). Two primers for each mutant were designed, where the forward primers 5' end contains the point mutation. After PCR, the amplicons were phosphorylated with T4 Polynucleotide Kinase (NEB), ligated with T4 DNA Ligase (NEB) and transformed into DH5alpha bacterial cells for amplification. Sanger sequencing was then used to

verify the identity of the point mutants. Double, triple and quadruple ELIC-pTLN mutant constructs were purchased from Twist Bioscience. The ELIC-pTLN constructs were linearized with MluI and transcribed from the SP6 promoter region. Capped ELIC cRNA was produced by *in vitro* transcription using the mMESSAGE mMACHINE SP6 kit (Ambion). The concentration of cRNA was determined using its absorbance at 260 nm. Additionally, the integrity of RNA was determined by agarose gel electrophoresis.

## 2.4 Electrophysiology

Stage V-VI *Xenopus laevis* oocytes were isolated as previously described (Laitko et al., 2006). To obtain optimal receptor expression, oocytes were injected with the indicated amount of cRNA for WT control and ELIC mutants (Table 1). Subsequently, oocytes were incubated for 1 to 4 days at 16℃ in $ND96^{+}$ buffer (5 mM HEPES, 96 mM NaCl, 2 mM KCl, 1 mM $MgCl_2$, 1 mM $CaCl_2$ and 2 mM pyruvate). After expression, injected oocytes were placed in a RC-1Z oocyte chamber (Harvard Apparatus; Hamden, CT) containing a buffer with a pH of 7.4 that is composed of 150 mM NaCl, 0.5 mM $BaCl_2$, 10 mM HEPES, and 1 mM DTT or 1 μM atropine if cysteamine or ACh was used in the experiment, respectively. The presence of DTT, a reducing agent, ensures that the sulfhydryl group of cysteamine is in the reduced thiol state. Atropine, a competitive antagonist to endogenous muscarinic AChRs, ensures ACh does not lead to the activation of endogenous channels such as calcium-activated chloride channels via muscarinic AChRs.

Once in the oocyte chamber, whole-cell currents were recorded using a two-electrode voltage-clamp apparatus (OC-725C oocyte clamp; Harvard Apparatus), whilst the appropriate

buffer solution flowed through the chamber at a rate of 5-10 mL/min. Currents through the plasma membrane, in response to various cysteamine and/or ACh concentrations, were measured with the transmembrane voltage clamped at -60 mV. The concentrations of cysteamine and ACh that were used varied for each mutant, spanning a range between 0.05 mM to 200 mM. Dose response curves for each mutant and WT were acquired from at least two different batches of oocytes.

**Table 1. Injection quantity and expression time of WT and mutant ELIC cRNA in *Xenopus laevis* oocytes.**

| ELIC Identity | Amount of RNA injected (ng) | Expression time (days) | n[a] |
|---|---|---|---|
| WT | 0.2 | 1 | 30 |
| Y38W | 2 | 1 | 23 |
| A75D | 2 | 1 | 23 |
| I79Y | 2 | 1 | 9 |
| F133W | 2 | 1 | 20 |
| A75D/F133W | 5 | 1 | 21 |

[a] Oocyte number reflects the sum of all the replicates done for each experiment in this thesis.

## 2.5 Data Analysis

For identifying a half maximal effective concentration ($EC_{50}$) and Hill coefficient of cysteamine, dose response curves were created by taking the magnitude of each cysteamine elicited peak current and normalizing this value to the maximal peak current. The log (base 10) cysteamine concentration in molar was then plotted on the x-axis against the fractional response on the y-axis. The data was fit using a nonlinear regression with a variable slope ($y = \frac{1}{1+10^{(\mathrm{LogEC50}-X)\times \mathrm{Hill\ Coefficient}}}$) sigmoidal dose response in GraphPad Prism. The individual $EC_{50}$ and Hill coefficients were averaged for each oocyte to derive a mean ± standard deviation. For identifying a half maximal inhibitory concentration ($IC_{50}$) and Hill coefficient of ACh, multiple solutions with the $EC_{50}$ of cysteamine were prepared in the presence of increasing ACh concentrations. The magnitude of each cysteamine-elicited peak current with increasing ACh concentrations, was normalized to the magnitude of the peak generated from an equivalent amount of cysteamine alone. Subsequent steps were the same as indicated above for deriving a cysteamine $EC_{50}$ and Hill coefficient. The individual $IC_{50}$ and Hill coefficients were averaged for each oocyte to derive a mean ± standard deviation.

Lastly, to identify the four normalized response values of WT and each mutant, 8 solutions were prepared. These solutions contain cysteamine at its measured 10% maximal effective concentration ($EC_{10}$), 20% maximal effective concentration ($EC_{20}$), $EC_{50}$ and 90% maximal effective concentration ($EC_{90}$), in the presence and absence of 25 mM ACh. The magnitude of each cysteamine-elicited peak current with 25 mM ACh, was normalized to the magnitude of the cysteamine-elicited peak current of the same cysteamine concentration without

25 mM ACh present (Figure 2.1). Complete ACh inhibition of the cysteamine-elicited response corresponds to a normalized response of 0, whilst no inhibition corresponds to 1.

Significance testing was done in GraphPad Prism using a one-way ANOVA followed by the Dunnett's post-hoc test, with a p value cutoff score below 0.01.

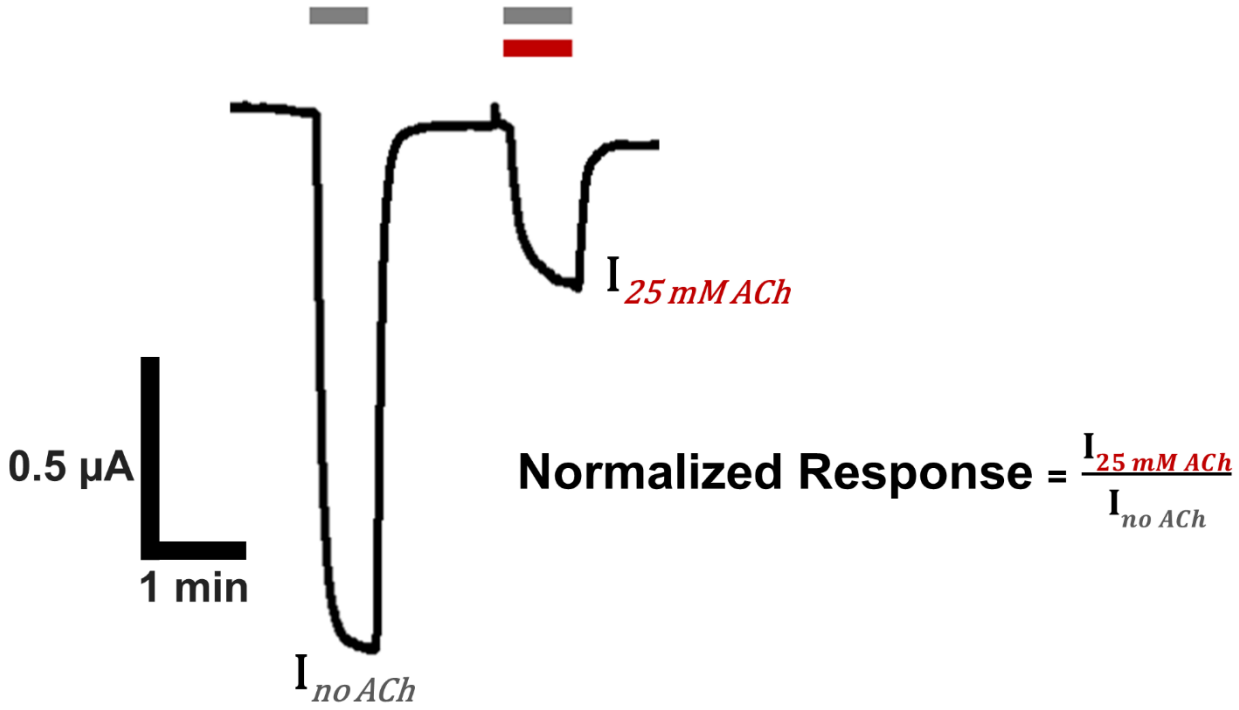


**Figure 2.1 Calculating the normalized response.**

A representative whole cell TEVC trace is shown, where the duration of cysteamine and ACh application is indicated in gray bars and red bars respectively. The same cysteamine concentration in the absence and presence of 25 mM ACh produces two peaks, corresponding to $I_{no\ ACh}$ and $I_{25mM\ ACh}$ respectively, of variable amplitude. The normalized response is then calculated.

# Chapter 3 - Results

## 3.1 Identifying ELIC Mutations Required to Install ACh Agonism

As mentioned above, ACh is an ELIC antagonist that binds to the orthosteric site without activating the channel. Presumably, this is because ELIC lacks a group of residues that can convert tight ACh binding to signal transduction, for effective opening of the transmembrane pore that leads to cation influx. However, the optimized group of residues in the AChBP can bind ACh with high affinity and undergo a conformational change that can activate an AChBP ECD – $5HT_{3A}$ TMD chimaera to conduct cations (Bouzat et al., 2004). To identify the location and composition of this optimized group of residues in the AChBP, we used SCA. First, a large and diverse ensemble of sequences homologous to the *Lymnaea stagnalis* AChBP were acquired and aligned. Then, the degree of coevolution between all positions in the MSA was calculated and plotted as a diagonally symmetric statistical coupling matrix. Information from this matrix was decomposed into three groups, or sectors, of amino acid residues (Figure 3.1A). Halabi et al. define four characteristics of sectors: "(1) statistical independence, (2) physical connectivity in the tertiary structure, (3) biochemical independence in mediating protein function, and (4) independent phenotypic variation in the protein family" (Halabi et al., 2009). The red sector in AChBP was the best candidate for carrying out the unique functional role of ACh agonism due to the presence of numerous well-characterized residues that are key for binding ACh, such as W53, D85, Y89 and W143 (Lee and Sine, 2004; Hansen et al., 2005; Brams et al., 2011; Olsen et al., 2014 ). In order to locate homologous red sector positions in ELIC, a structural superposition was used to perform the alignment with the *Lymnaea stagnalis* AChBP (Appendix Figure 4.1). The mapped red sector positions in ELIC differed in composition, suggesting 15 mutations that are required to install this sector for ACh activity (Figure 3.1B). To prevent the large structural perturbation that would be caused by installing the entire sector of residues, only four positions

out of the 15 were selected for mutagenesis. The four positions were selected based on the proximity of the residue to ACh in the ELIC-ACh complex structure (Pan et al., 2012; Figure 3.1B). Another criterion for selecting these four positions for mutagenesis was that the corresponding AChBP residues, which are conserved in AChRs, have been previously implicated in ACh agonism. Three of the four residues are I79, Y38 and F133, which correspond to Y89, W53 and W143 in the AChBP that form strong hydrogen bonding and cation-π interactions with the quaternary amine of ACh (Olsen et al., 2014). The fourth residue is A75, which corresponds to D85 in the AChBP that, indirectly, through a hydrogen bond linkage with W143, influences ACh binding (Lee and Sine, 2004). First, to understand whether individual point mutants can lead to ACh agonism, the Y38W, A75D, I79Y and F133W mutations were tested.

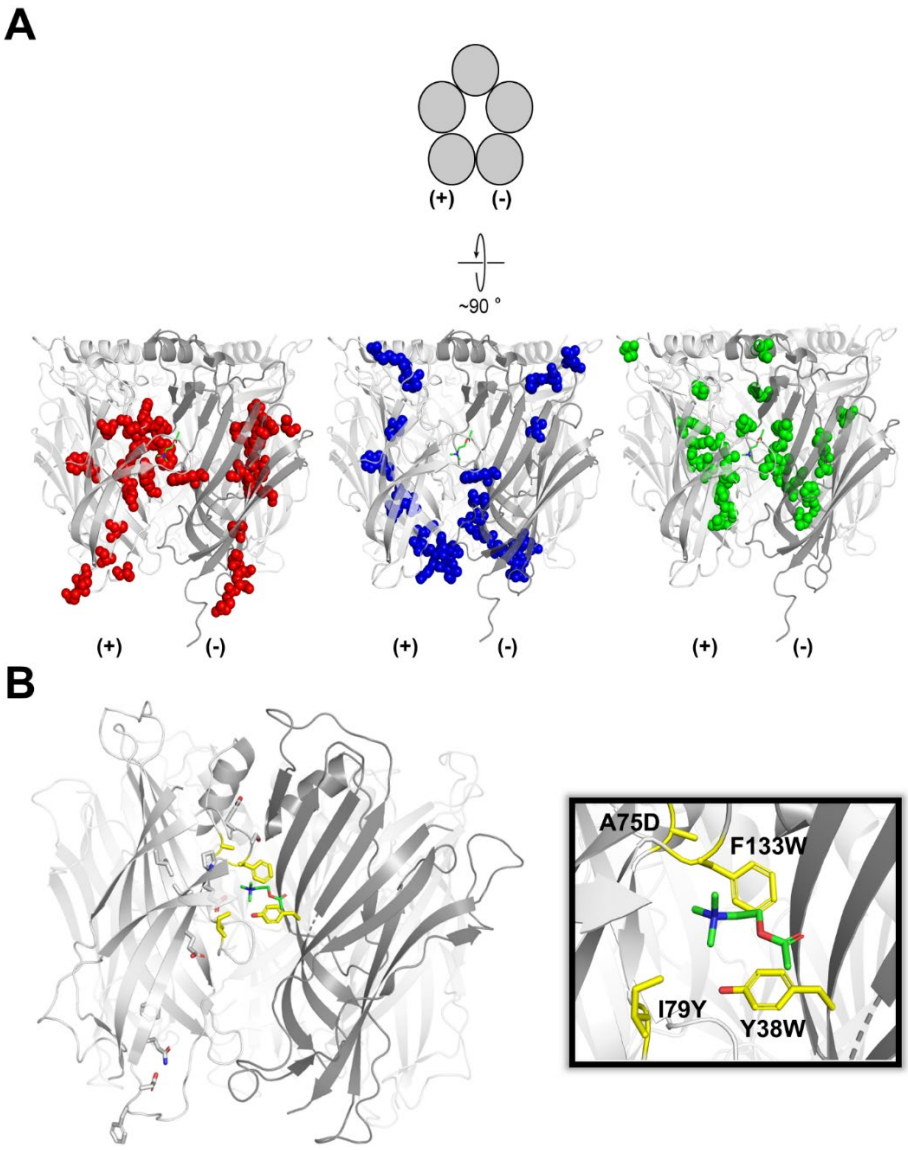


**Figure 3.1 Statistical coupling analysis of AChBPs and mapping red sector positions onto ELIC.** (A) A top-down view of an AChBP homopentamer is presented as gray circles highlighting the orientation of the principal (+) and complementary (-) subunits. The *Lymnaea stagnalis* AChBP (PDB: 3WIP) side-view is presented below showing the three SCA sectors as spheres in red, blue and green. Each sector is depicted on both the principal and complementary subunits. The red sector is composed of residues: W53, D85, Y89, S126, E131, S132, A134, C136, K139, I140, G141, S142, W143, T144, H145, S147, S151. The blue sector is composed of residues: P20, T21, R23, V29, N37, E40, V41, N42, E43, I44, T45, N46, D49, V50, V51, W53. Lastly, the green sector is composed of residues: V48, S67, P77, L86, A87, A88, Y113, P115, S116, I117, Q119, F121, T144. (B) The left image is a side-view representation as in (A) of ELIC crystallized with ACh (PDB: 3RQW) where the red sector positions from AChBP are mapped onto ELIC. The corresponding residues at homologous positions in ELIC are shown as sticks on the principal subunit consisting of: A75, I79, F121, D122, Q124, F126, E129, L130, E131, P132, F133, S134, Y135, L140, except for residue Y38 which is shown on the complementary subunit only. The red sector residues and ACh nitrogen and oxygen atoms are coloured in blue and red respectively. Carbon atoms are shown in yellow, gray and green to differentiate between the residues used for mutagenesis, other red sector residues and acetylcholine respectively. The right image is a close-up view of the active site containing the residues in ELIC that were mutated to their AChBP identity. For clarity the C-loop has been removed.

## 3.2 Single ELIC Point Mutations Decrease Cysteamine Potency Without Altering Agonist Specificity

We began by examining the effects of each substitution on cysteamine agonism. All the single mutant ELIC receptors expressed in *Xenopus* oocytes, and upon successive addition of increasing cysteamine concentrations, we observed progressively larger peak currents (Figure 3.2A i-v). By plotting the relative peak current as a function of the log (base 10) cysteamine concentration and fitting the resulting relationship using a nonlinear regression, a sigmoidal dose response curve was obtained (Figure 3.2B). From this dose response curve, we identified an $EC_{50}$ of cysteamine for each mutant and WT (Table 2).

The $EC_{50}$ of cysteamine in the WT-receptor was determined to be 0.6 ± 0.1 mM with a Hill coefficient of 2.6 ± 0.4, which is consistent with the previously reported values of 0.37 mM and 2.7, respectively (Zimmermann and Dutzler, 2011; Table 2). In comparison to WT-ELIC, the cysteamine potency of the Y38W mutant was unchanged, while A75D and F133W resulted in a significant loss-of-function corresponding to a 3-fold and 7-fold difference, respectively (Figure 3.2B). This 3-fold and 7-fold loss-of-function corresponds to an $EC_{50}$ increase, from 0.6 ± 0.1 mM in the WT receptor to 1.6 ± 0.4 mM for A75D, and to 4.3 ± 0.6 mM for F133W (Table 2). A significant loss-of-function for the A75D mutation suggests that, despite its distance from the agonist, position 75 serves a functionally important role in channel activation (Table 2). Y38W was the only mutation that significantly altered the Hill coefficient from 2.6 ± 0.4 in the WT receptor to 1.4 ± 0.2 (Table 2).

Slow macroscopic channel activation, slow channel desensitization or both was observed for the I79Y mutant with 5 mM cysteamine, which is unique from the other single mutants and

WT-ELIC (Appendix Figure 4.2). Due to this slow activation, obtaining a dose response curve from a range of cysteamine concentrations was impractical. To resolve this, a fixed interval of 30 seconds was chosen for cysteamine application. When testing a range of cysteamine concentrations, each applied for 30 seconds, the magnitude of cysteamine-induced currents appeared to saturate at 50 mM (Figure 3.2A iv). From this, a pseudo-dose response curve and the corresponding $EC_{50}$ of 13.8 ± 1.0 mM were generated; this represents a 24-fold increase in cysteamine $EC_{50}$ in comparison to WT (Figure 3.2B, Table 2).

We next explored whether ACh could activate these single mutant ELIC receptors. Successive addition of ACh at a concentration of 0.5 mM to 50 mM was followed by application of 5 mM cysteamine (Appendix Figure 4.2). This 5 mM cysteamine application was used to ensure that functional receptors were sufficiently expressed in oocytes. None of the single mutants nor WT-ELIC produced any peak current when ACh was applied, whilst the application of 5 mM cysteamine produced a large and robust peak current (Appendix Figure 4.2). Given the absence of ACh agonism in these single mutants, we further investigated whether there were alterations to the potency with which ACh could inhibit the receptor.

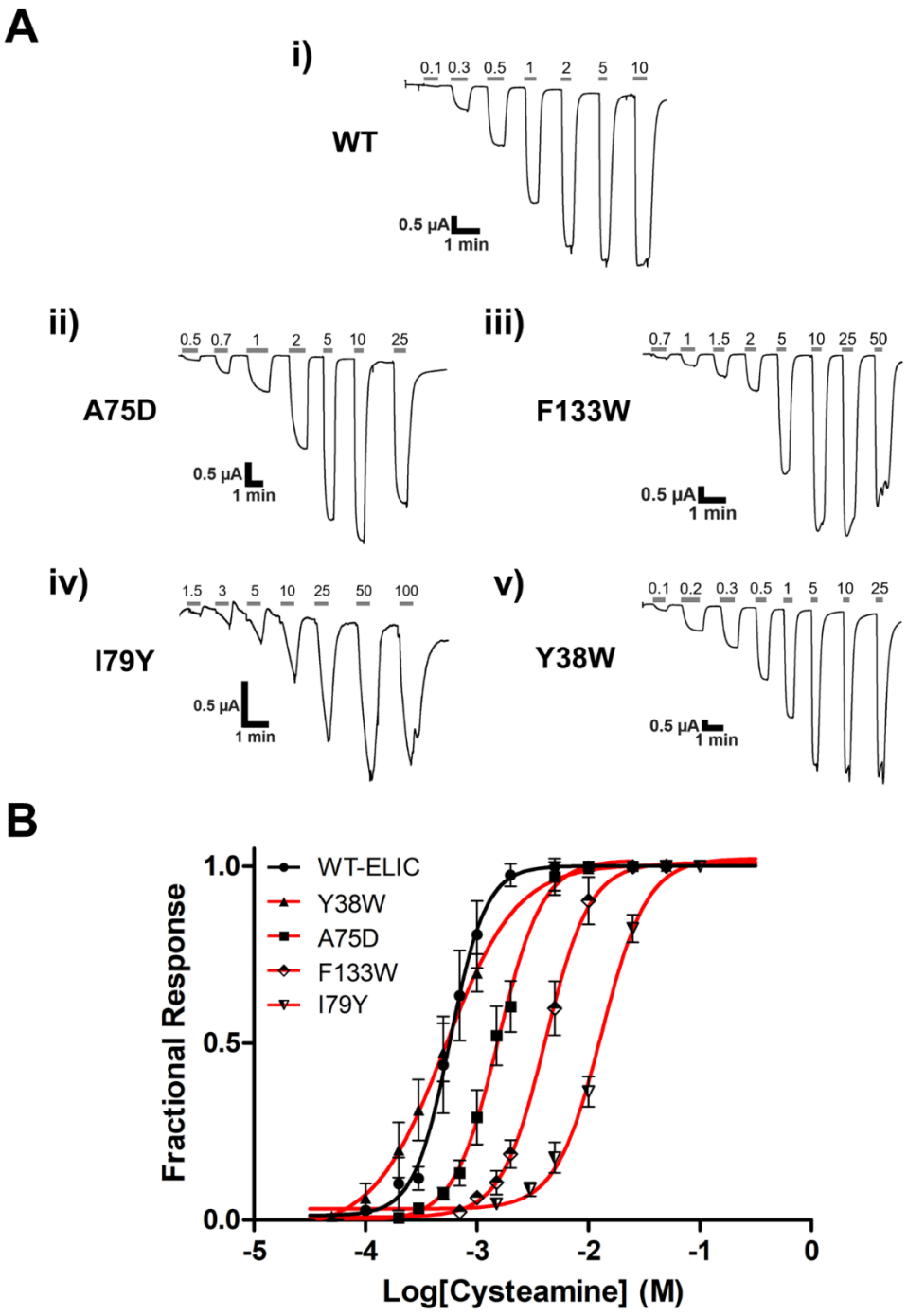


**Figure 3.2 Single mutant TEVC traces and dose response curves for cysteamine activation.**

(A) Representative whole cell TEVC traces are provided for the single mutants (ii-v) and WT receptor (i). The cysteamine concentrations (mM) that were used are indicated above each peak. The duration of cysteamine application is shown in gray bars, with the time in-between application representing a washing step that removes cysteamine and returns the channels to a baseline signal. (B) The average dose response curves of WT-ELIC (black curve with black circles), Y38W (red curve with black triangles), A75D (red curve with black squares), F133W (red curve with black and white diamonds), and I79Y (red curve with black and white inverted triangles) are shown. Error bars represent standard deviation with $n \geq 6$ oocyte replicates.

**Table 2. Cysteamine potency of single ELIC mutants.**

| ELIC Identity | Cysteamine $EC_{50}$ (mM)[a] | Hill Coefficient[a] | n | Fold Attenuation[e] |
|---|---|---|---|---|
| WT | 0.6 ± 0.1 | 2.6 ± 0.4 | 11 | -- |
| Y38W | 0.5 ± 0.1 | 1.4 ± 0.2[d] | 8 | 1 |
| A75D | 1.6 ± 0.4[c] | 2.3 ± 0.5 | 9 | 3 |
| I79Y[b] | 13.8 ± 1.0[c] | 2.2 ± 0.3 | 6 | 24 |
| F133W | 4.3 ± 0.6[c] | 2.3 ± 0.3 | 8 | 7 |

[a] Data was acquired after 1 day of expression. The individual $EC_{50}$ and Hill coefficients of each oocyte were averaged to derive the reported mean ± standard deviation.
[b] Estimate of $EC_{50}$ and Hill coefficient are provided based on cysteamine application for 30 sec in the range of 1.5 mM to 100 mM.
[c] $p < 0.001$ relative to WT $EC_{50}$ done with a one-way ANOVA followed by Dunnett's post-hoc test.
[d] $p < 0.001$ relative to WT Hill coefficient done with a one-way ANOVA followed by Dunnett's post-hoc test.
[e] Mutant $EC_{50}$ divided by WT $EC_{50}$ rounded to the nearest whole number.

## 3.3 Acetylcholine's Potency as an Inhibitor is Altered in the Single Point Mutations

None of the single mutations enabled channel activation by ACh; however, the cysteamine $EC_{50}$ was significantly decreased for all of the mutants, excluding Y38W (Appendix Figure 4.2, Table 2). We next investigated the effect of each substitution on ACh antagonism. In the WT and single mutant ELIC receptors, a fixed cysteamine concentration, corresponding to the $EC_{50}$ of each receptor, was used to activate the channel. This initial peak current produced by cysteamine alone became progressively smaller upon successive applications of increasing concentrations of ACh in the presence of cysteamine maintained at the $EC_{50}$ (Figure 3.3A). The single ELIC mutants are thus also inhibited by ACh, but to different degrees. By plotting the relative peak current as a function of the log (base 10) ACh concentration and fitting the resulting relationship using a nonlinear regression, a sigmoidal dose response curve was obtained (Figure 3.3B). From this dose response curve, an $IC_{50}$ of ACh was identified (Table 3).

The $IC_{50}$ of ACh in the WT receptor was determined to be 1.1 ± 0.4 mM, which is consistent with the previously reported value of 1.4 mM, captured in the presence of cysteamine at the $EC_{60}$ instead of $EC_{50}$ (Pan et al., 2012; Table 3). The only mutant that appears to decrease the $IC_{50}$ of ACh inhibition is Y38W, with a decrease from 1.1 ± 0.4 mM to 0.4 ± 0.1 mM (Table 3, Figure 3.3B). However, this difference in ACh $IC_{50}$ between WT and Y38W is not statistically significant (Table 3). Y38W was the only mutant with a change in Hill coefficient compared to WT that was significant, with an increase from -1.3 ± 0.3 to -1.7 ± 0.2 (Table 3).

The mutations A75D and F133W produced a roughly 10-fold increase in ACh $IC_{50}$, with no significant change in Hill coefficient relative to WT (Table 3, Figure 3.3B). Concentrations as

high as 100 mM of ACh were not sufficient to fully inhibit the cysteamine-induced peaks of these two mutants (Figure 3.3A iii-iv). The most striking mutation is A75D, which does not directly contact cysteamine or ACh; however, it has a functional impact on cysteamine agonism and ACh inhibition. To determine if ACh inhibition could be further reduced, we combined the A75D mutation with F133W.

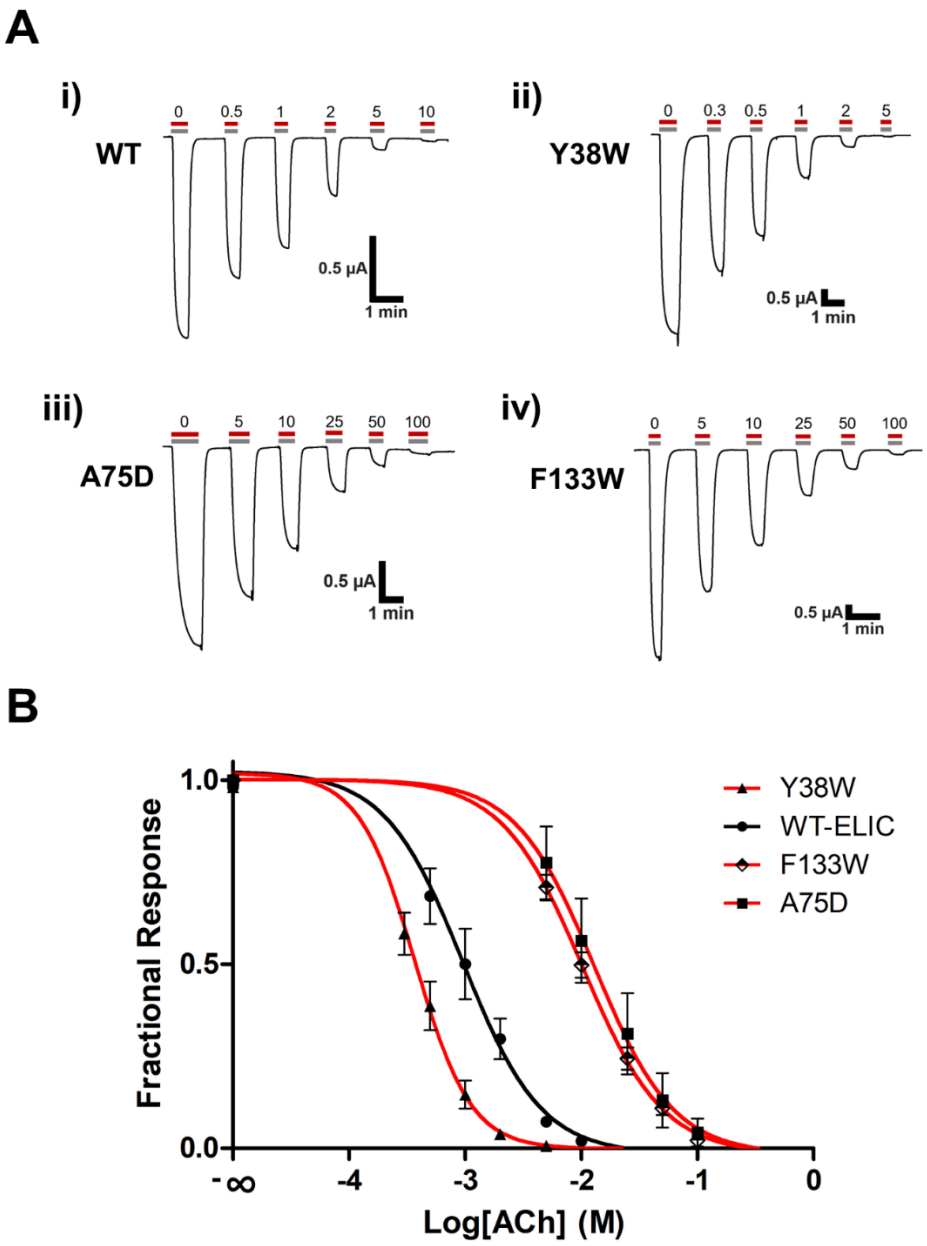


**Figure 3.3 Comparing ACh inhibition between single point mutants.**

(A) Representative whole cell TEVC traces are provided for the single mutants (ii-iv) and WT receptor (i). A fixed cysteamine $EC_{50}$ of each mutant was used in combination with the indicated ACh concentrations (mM) above each peak. The duration of cysteamine and ACh co-application is shown in gray bar and red bars respectively, with the time in-between application representing a washing step that removes the ligands and returns the channels to a baseline signal. (B) The average dose response curves of WT-ELIC (black curve with black circles), Y38W (red curve with black triangles), A75D (red curve with black squares) and F133W (red curve with black and white diamonds) are shown. Error bars represent standard deviation with $n \geq 5$ oocyte replicates. The y-intercept corresponds to a 1.0 fractional response generated from the initial cysteamine peak with no ACh present.

**Table 3. Potency of ACh inhibition in the single ELIC mutants.**

| ELIC Identity | ACh $IC_{50}$ (mM)[a] | Hill Coefficient[a] | n | Fold Attenuation[d] |
|---|---|---|---|---|
| WT | 1.1 ± 0.4 | -1.3 ± 0.3 | 9 | -- |
| Y38W | 0.4 ± 0.1 | -1.7 ± 0.2[c] | 8 | 0.4 |
| A75D | 12.4 ± 2.8[b] | -1.3 ± 0.2 | 5 | 11 |
| F133W | 11.1 ± 1.3[b] | -1.2 ± 0.1 | 5 | 10 |

[a] Data was acquired after 1 day of expression. The individual $IC_{50}$ and Hill coefficients of each oocyte were averaged to derive the reported mean ± standard deviation.
[b] $p < 0.001$ relative to WT $IC_{50}$ done with a one-way ANOVA followed by Dunnett's post-hoc test.
[c] $p < 0.01$ relative to WT Hill coefficient done with a one-way ANOVA followed by Dunnett's post-hoc test.
[d] Mutant $IC_{50}$ divided by WT $IC_{50}$ rounded to two significant figures.

## 3.4 The A75D/F133W Double Mutant Abolishes ACh Inhibition

The A75D and F133W single mutants each independently led to reduced inhibition by ACh. To identify whether ACh inhibition could be further reduced, these two substitutions were combined to form the A75D/F133W double mutant. The double mutant expressed in *Xenopus* oocytes, and upon successive addition of increasing cysteamine concentrations, progressively larger peak currents were observed (Figure 3.4A). In comparison to its constituent single mutants, the double mutant A75D/F133W produced a near-additive change in cysteamine potency. This was a 12-fold increase in cysteamine $EC_{50}$ in comparison to WT, which corresponds to a concentration of 6.9 ± 0.7 mM (Table 4, Figure 3.4A). A significant increase in Hill coefficient was seen for A75D/F133W, with a value of 3.8 ± 0.3 in comparison to 2.6 ± 0.4 in the WT (Table 4).

Next, a cysteamine concentration corresponding to the $EC_{50}$ of the A75D/F133W double mutant was used to activate the channel. Unlike the WT or corresponding single mutants, the initial peak current produced by cysteamine alone was not progressively diminished upon successive application of increasing ACh concentrations, in the presence of a fixed cysteamine $EC_{50}$ (Figure 3.4B). The A75D/F133W double mutant appeared to abolish ACh's function as an inhibitor. Instead of inhibiting the cysteamine-induced response, concentrations as high as 100 mM of ACh increased or potentiated the $EC_{50}$ cysteamine peak current (Figure 3.4B).

The resulting potentiated current in the presence of ACh is within a single standard deviation from the peak current in its absence (Figure 3.4B). Due to variability between oocytes and confounding variables such as channel desensitization and run-down, the ACh induced channel potentiation could not be further characterized from this experiment (Figure 3.4B). To

further investigate the function of ACh on this A75D/F133W double mutant receptor, and to understand the cysteamine concentration dependence of ACh inhibition for the single point mutations, an additional experiment was performed.

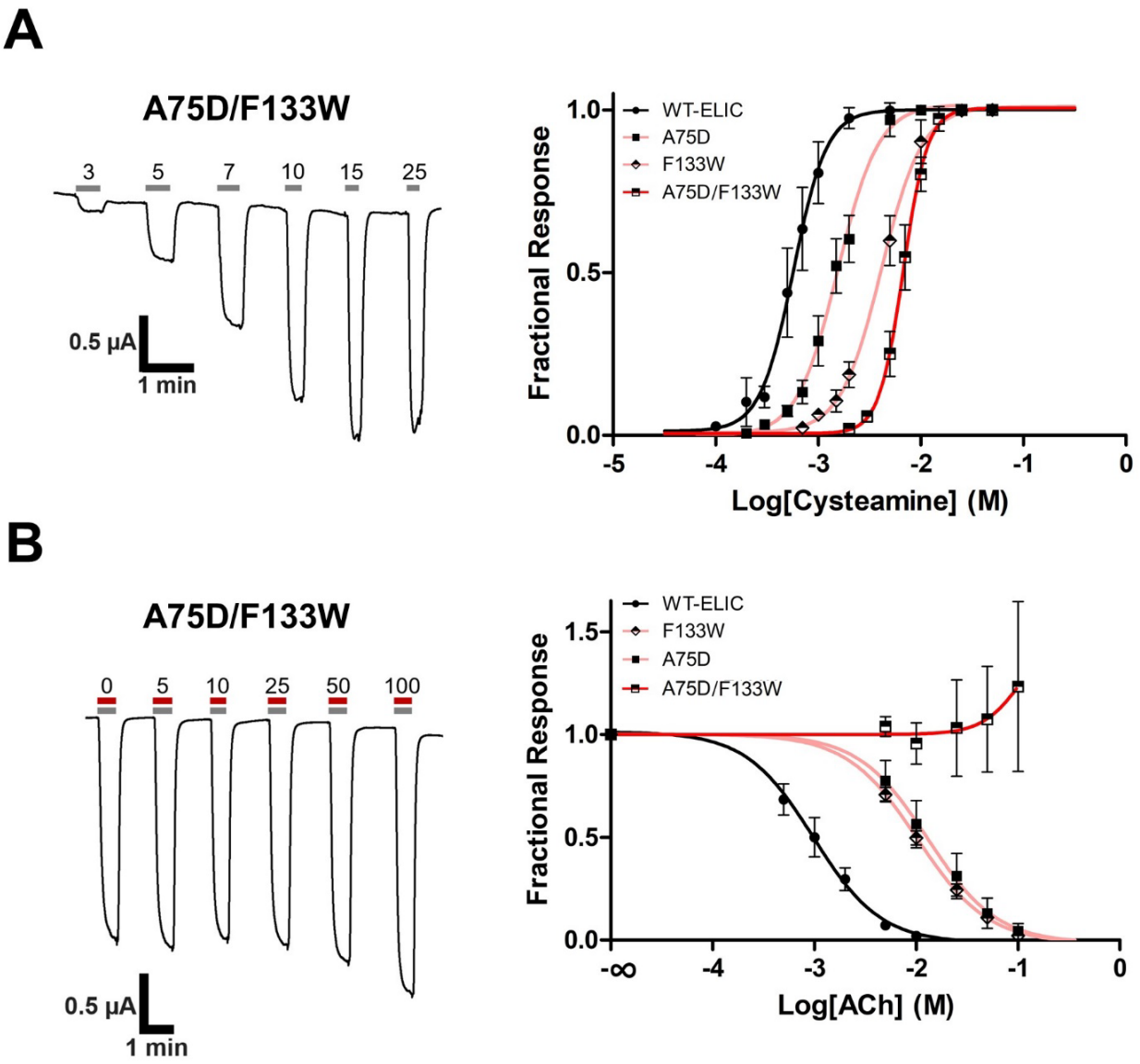


**Figure 3.4 Characterizing the cysteamine activation and ACh inhibition of the A75D/F133W double mutant.**

(A) On the left, a representative whole cell TEVC trace is provided for the A75D/F133W double mutant. Cysteamine concentrations (mM) are indicated above each peak with the duration of cysteamine application shown in gray bars. The time in-between application represents a washing step that removes cysteamine and returns the channels to a baseline signal. On the right, the average dose response curves of WT-ELIC (black curve with black circles), F133W (pink curve with black and white diamonds), A75D (pink curve with black squares) and A75D/F133W (red curve with black and white squares) are shown. Error bars represent standard deviation with $n \geq 7$ oocyte replicates. (B) On the left, a similar TEVC trace as in A is shown, however here the concentration of cysteamine at the $EC_{50}$ value of A75D/F133W is used in combination with the indicated ACh concentrations (mM) above each peak. The duration of ACh application is shown in red bars. On the right, the average dose response curves of WT-ELIC (black curve with black circles), F133W (pink curve with black and white diamonds), A75D (pink curve with black squares) and A75D/F133W (red curve with black and white squares) are shown. Error bars represent standard deviation with $n \geq 5$ oocytes. The y-intercept corresponds to a 1.0 fractional response generated from the initial cysteamine peak with no ACh present. Note the dose response curves in A and B for the A75D and F133W mutants are from Figure 3.2 and Figure 3.3 but are instead highlighted in pink.

**Table 4. Cysteamine potency of the A75D/F133W double mutant.**

| ELIC Identity | Cysteamine $EC_{50}$ (mM)[a] | Hill Coefficient[a] | n | Fold Attenuation[d] |
|---|---|---|---|---|
| WT | 0.6 ± 0.1 | 2.6 ± 0.4 | 11 | -- |
| A75D/F133W | 6.9 ± 0.7[b] | 3.8 ± 0.3[c] | 7 | 12 |

[a] Data was acquired after 1 day of expression. The individual $EC_{50}$ and Hill coefficients of each oocyte were averaged to derive the reported mean ± standard deviation.
[b] $p < 0.001$ relative to WT $EC_{50}$ done with a one-way ANOVA followed by Dunnett's post-hoc test.
[c] $p < 0.001$ relative to WT Hill coefficient done with a one-way ANOVA followed by Dunnett's post-hoc test.
[d] Mutant $EC_{50}$ divided by WT $EC_{50}$ rounded to the nearest whole number.

## 3.5 The A75D/F133W Double Mutant can Convert ACh from a Competitive Antagonist to a Potentiator

Up to this point, the shifted potency of ACh as an inhibitor has been characterized in the presence of the $EC_{50}$ of cysteamine for A75D/F133W and the corresponding single mutants. To gain insight into the cysteamine concentration dependence of ACh inhibition, the $EC_{10}$, $EC_{20}$, $EC_{50}$ and $EC_{90}$ of cysteamine were used with and without excess ACh. These cysteamine concentrations are representative of the dose response range for each mutant. Additionally, an excess ACh concentration of 25 mM was chosen to best highlight the distinct effect of ACh in the WT versus mutant receptors.

By comparing the magnitude of the peak current with both cysteamine and 25 mM ACh present to the peak current with only cysteamine present, a normalized response can be determined (Figure 2.1). A range of cysteamine concentrations produced currents that were almost entirely inhibited in the WT and Y38W receptors with 25 mM ACh (Figure 3.5A, Figure 3.5B). In the F133W mutant, it is evident that increasing the cysteamine concentration from 1.6 mM or 2.3 mM to 4.3 mM and 11.3 mM reduces the amount of inhibition that 25 mM ACh elicits (Table 5, Figure 3.5B). For the A75D mutant, the most pronounced difference in ACh inhibition is evident between the first three cysteamine concentrations of 0.6 mM, 0.9 mM, 1.6 mM versus the highest concentration at 4.2 mM. At 4.2 mM of cysteamine, ACh produces a normalized response of $0.84 \pm 0.05$, which is approaching the uninhibited cysteamine peak current of A75D receptors (Table 5, Figure 3.5B). From the previous experiment, the A75D/F133W double mutant, in the presence of $EC_{50}$ or 6.90 mM cysteamine, was resistant to ACh inhibition. By directly comparing the cysteamine elicited peak current in the absence and presence of 25 mM ACh, it is clear that ACh is in fact potentiating the agonist evoked response

(Figure 3.5A). This potentiation is cysteamine concentration dependent, where currents induced by lower cysteamine concentrations are less potentiated by ACh (Figure 3.5B). A significant increase in peak current with ACh, in comparison to a baseline signal of 1.0 (corresponding to the peak current without ACh), is present at the $EC_{20}$, $EC_{50}$ and $EC_{90}$ normalized response values (Table 5).

In the F133W and A75D single mutants, increasing the cysteamine concentration reduces the amount of inhibition elicited by 25 mM ACh. However, in the double mutant, A75D/F133W, increasing cysteamine concentration further amplifies the ACh-induced potentiation. Lastly, this strikingly different role of ACh in the WT and A75D/F133W double mutant receptors was compared (Figure 3.6). In the WT-receptor, 25 mM ACh with $EC_{50}$ cysteamine almost fully reduces the cysteamine induced peak to baseline, demonstrating the essentially complete inhibition of the cysteamine-induced current. In stark contrast, for the double mutant, the same 25 mM ACh pulse in the presence of $EC_{50}$ cysteamine instead increases the cysteamine-induced current. Thus, rather than acting as a competitive inhibitor, ACh instead potentiates agonist induced currents of the double mutant.

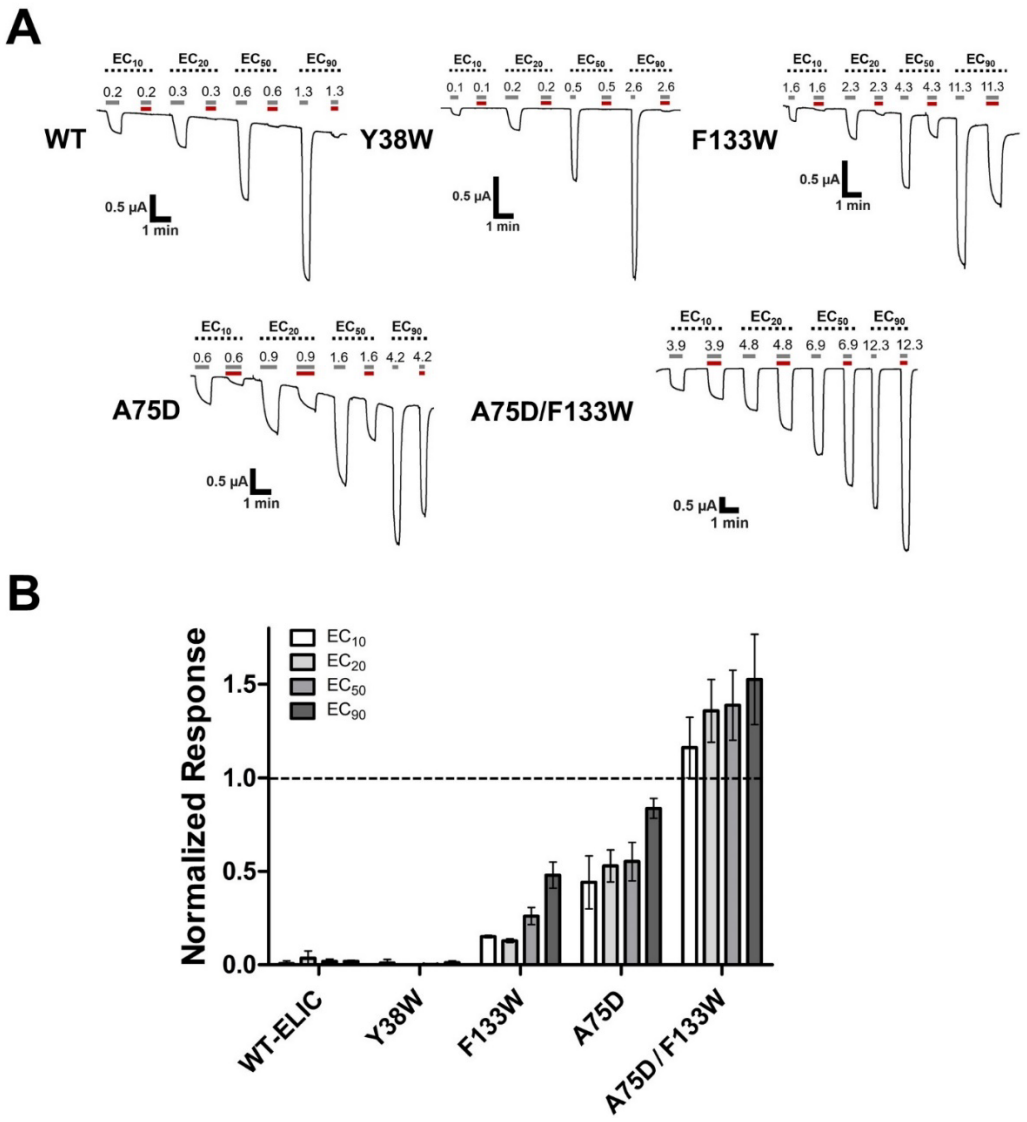


**Figure 3.5 The cysteamine concentration dependence of ACh inhibition or potentiation in the single and A75D/F133W double ELIC mutants, respectively.**

(A) Representative whole cell TEVC traces of WT, Y38W, A75D, F133W and A75D/F133W ELIC. The cysteamine concentrations (mM) corresponding to the $EC_{10}$, $EC_{20}$, $EC_{50}$ and $EC_{90}$ of each mutant and WT are indicated above each peak. A cysteamine pulse was first applied to identify a peak current following an ACh co-application where 25 mM of ACh was used in combination with the same cysteamine concentration applied directly prior. This was repeated for a range of four cysteamine concentrations. The duration of cysteamine application is shown in gray bars with ACh application in red bars. The time in-between application represents a washing step that removes ligands and returns the channels to a baseline signal. (B) The traces from A were used to calculate a Normalized Response which is shown on the y-axis where Normalized Response = $I_{25\ mM\ ACh}/I_{no\ ACh}$. This equation corresponds to the relative magnitude of the peak current with 25 mM ACh and cysteamine present ($I_{25\ mM\ ACh}$) versus the peak current with only cysteamine present ($I_{no\ ACh}$). The Normalized Response is plotted against the identity of each receptor on the x-axis. In the absence of ACh inhibition $I_{25\ mM\ ACh}$ would be equal to $I_{no\ ACh}$, which is represented as a dashed horizontal line with a Normalize Response of 1.0. Each receptor was characterized with 4 cysteamine concentrations shown in white bars, light gray bars, dark gray bars and black bars corresponding to the $EC_{10}$, $EC_{20}$, $EC_{50}$ and $EC_{90}$ of cysteamine respectively. Error bars represent standard deviation with $n \geq 4$ oocytes.

**Table 5. ACh attenuated or potentiated cysteamine response in the WT, single and A75D/F133W double ELIC mutants.**

| ELIC Identity | $EC_{10}$ Normalized Response[a] | $EC_{20}$ Normalized Response[a] | $EC_{50}$ Normalized Response[a] | $EC_{90}$ Normalized Response[a] | n |
|---|---|---|---|---|---|
| WT | 0.01 ± 0.02 | 0.04 ± 0.04 | 0.02 ± 0.01 | 0.02 ± 0.01 | 5 |
| Y38W | 0.01 ± 0.02 | 0 ± 0 | 0 ± 0 | 0.01 ± 0.01 | 4 |
| A75D | 0.44 ± 0.14 | 0.53 ± 0.09 | 0.55 ± 0.10 | 0.84 ± 0.05 | 6 |
| F133W | 0.15 ± 0.01 | 0.13 ± 0.01 | 0.26 ± 0.05 | 0.48 ± 0.07 | 4 |
| A75D/F133W | 1.16 ± 0.16 | 1.36 ± 0.17[b] | 1.39 ± 0.19[b] | 1.53 ± 0.24[b] | 4 |

[a] Data was acquired after 1 day of expression. The individual Normalized Response of the specific cysteamine concentration was averaged across each oocyte to derive the reported mean ± standard deviation. Two TEVC current peaks were used to calculate Normalized Response, one generated from applying 25 mM ACh with the indicated EC cysteamine. The other from only the EC cysteamine alone.

[b] $p < 0.01$ relative to a Normalized Response of 1.0 done with a one-way ANOVA followed by Dunnett's post-hoc test.

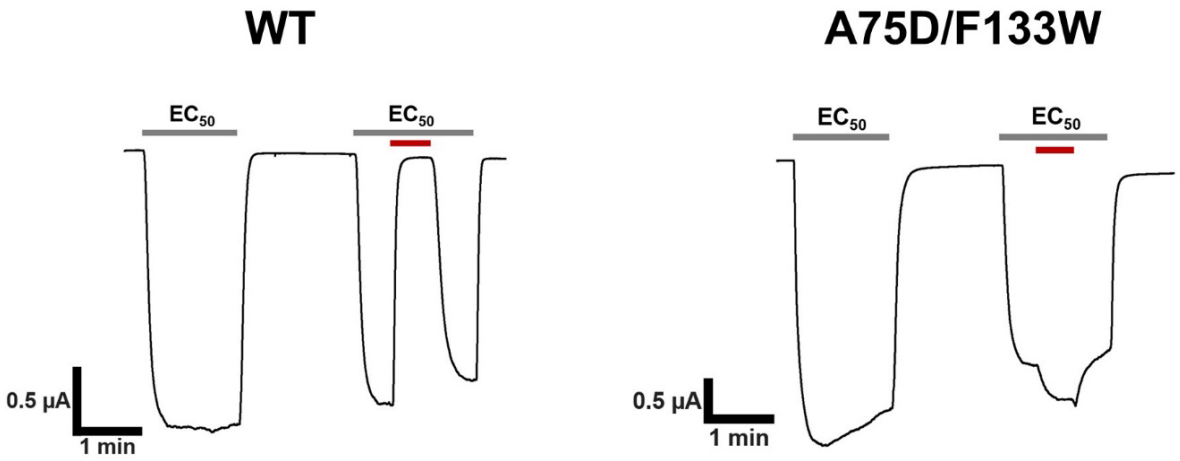


**Figure 3.6 Contrasting the role of ACh in WT versus A75D/F133W double mutant ELIC receptors.**

Whole cell TEVC traces of WT and A75D/F133W ELIC are shown above. In both WT and double mutant, a 2-minute (gray bar) cysteamine pulse was applied following a washing step to remove cysteamine and return the channels to a baseline signal. The second peak consists of a 40-sec cysteamine $EC_{50}$ pulse followed by a 40-sec 25 mM ACh with $EC_{50}$ cysteamine pulse and finally a 40-sec $EC_{50}$ cysteamine pulse. Following this second peak a washing step was included returning the channels to a baseline signal.

# Chapter 4 - Discussion

ELIC, a prokaryotic pLGIC, is activated by primary amines and competitively inhibited by ACh (Zimmermann and Dutzler, 2011; Pan et al., 2012). We set out to change ACh from a competitive antagonist into an agonist, and thus gain insight into agonism in this model pLGIC. Using SCA, we identified a sector of residues involved in ACh binding and in allostery in the related AChBP. Mapping this sector of residues onto ELIC led to the identification of four candidate residues important for ACh binding and allostery. Substituting AChBP residues for the ELIC residues at these four sites led to four single and one double mutant that altered the potency of ACh as an inhibitor, as well as the potency of cysteamine as an agonist. While none of these substitutions converted ACh into an ELIC agonist, the double mutant A75D/F133W abolished the antagonist activity of ACh, and instead converted ACh into a potentiator of cysteamine-activated currents.

An agonist is a ligand that can both bind and induce channel opening of an ion channel. The first requirement of an agonist is to diffuse into the binding site and make key contacts with the receptor. In ELIC, small unbranched primary amines are capable of binding and interacting with the receptors in such a way that leads to full channel activation (Zimmermann and Dutzler, 2012). The nAChRs, which are formed by a combination of 17 different AChR subunits, contain members with different agonist specificities. For example, the native GABA receptor agonist, GABA, can fully activate ELIC and partially activate the muscle-type nAChR, but not the α7 nAChR (Spurny et al., 2012; Dionisio et al., 2015). Similarly, a drug treatment used for Alzheimer's disease, MXB-A (GST-21), is a partial agonist of the α7 nAChR, but also a potent antagonist of α4β2 nAChR (Rollema et al., 2010). All nAChRs are fully activated by ACh and generally contain conserved binding site residues in the principal subunit. Thus, the basis by which certain agonists are discriminated against are subtle. Generally, the agonist binding sites

of pLGICs are abundant in aromatic residues that form an aromatic box around the agonist amine group. The side chains of these aromatic residues form at least one cation-π interaction that imposes stringent geometric constraints on the agonist (Gallivan and Dougherty, 1999). Despite the similarity between the nAChR and ELIC binding site, key residue discrepancies are present. Two glutamic acids, E131 and E77 form electrostatic contact with the amine portion of the agonist in ELIC, which are absent in nAChRs. Instead, nAChRs such as the muscle-type nAChR, contain more electron rich tryptophan residues homologous to position Y38 and F133 in ELIC. Additionally, a key tyrosine in the nAChRs, homologous to I79 in ELIC, forms a hydrogen bond with the agonist amine group. After binding and forming interactions with residues in the orthosteric site, an agonist induces a conformational change that opens the transmembrane domain pore for ion conductance. Residues involved in linking binding to gating, in addition to distal residues that impact binding affinity, are not well characterized. The fact that ACh binds with comparable affinity to native ELIC agonists, but instead acts as a competitive antagonist, presented a great opportunity to study the determinants of agonism (Pan et al., 2012). By taking a synthetic approach, we attempted to convert ELIC into an ACh activated receptor, to understand the complex amino acid determinants that discern an antagonist from an agonist. The approach we used is SCA, which is well-suited for identifying sectors, or groups of residues that carry out an independent function, such as agonism. A sector presumably would contain residues not only in direct contact with the agonist, but additional residues that are involved in indirect binding and linking agonist binding to channel gating. Transplanting portions of a sector, or the entire sector responsible for ACh agonism, from a nAChR or AChBP into ELIC would introduce key residues whose significance for agonism is not obvious by structure gazing.

We performed SCA on the AChBP rather than a full nAChR, due to the presence of a high-resolution crystal structure of the *Ls*-AChBP bound to ACh. A 2.6 Å crystal structure of *Ls*-AChBP was solved with five ACh molecules bound in total at the five orthosteric sites (Olsen et al., 2014). The crystal structure of ELIC solved at 2.9 Å with ACh bound also happened to have a total of five ACh molecules bound at the five orthosteric sites. The high resolution AChBP structure and the presence of ACh at each orthosteric site were crucial for the initial Rosetta 3.9 protein design. These designed sequences were the same length and 3D structure as *Ls*-AChBP bound to ACh, allowing us to build a profile HMM for querying thousands of similar sequences. The resulting sequences that were queried had to resemble the 3D structure of AChBP bound to ACh. In the future, it would be informative to perform SCA on the more recent nAChR structure that was not available when we embarked upon this work (Rahman et al., 2020), to reveal all of the residues that are key for ACh agonism, from the orthosteric site to the channel gate.

Out of the three sectors, the red sector positions that were identified in the AChBP and subsequently mapped in ELIC and the muscle-type nAChR contained well-established residues that are crucial for agonism in these two pLGICs. Statistical coupling analysis is a method that identifies groups of co-evolving amino acids, which are connected in the tertiary structure, with each group serving a distinct functional role in the protein (Halabi et al., 2009). In the S1A serine protease family, three sectors were identified, with each sector independently affecting catalytic activity, thermal stability, and catalytic specificity of the enzyme (Halabi et al., 2009). Consequentially, these sector positions are sensitive to mutagenesis, whilst non-sector positions are more tolerant. In the case of the PDZ domain, it was established that only two mutations within a sector were sufficient to switch the specificity of this protein towards a class-switching ligand (McLaughlin et al., 2012). The red sector contained a number of residues that had already

been implicated in ACh agonism of related AChRs. This suggested that the red sector may serve the independent functional role of agonism. The red sector contained residues W53, D85, Y89, K139 and W143, which correspond to γW55/δW57, αD89, αY93, αK145 and αW149 in the muscle-type nAChR; all of these are key for ACh agonism (Zhong et al., 1998; Karlin, 2002; Celie et al., 2004; Lee and Sine, 2004; Mukhtasimova et al., 2005; Li et al., 2011; Olsen et al., 2014) (Appendix Figure 4.1 and Results Figure 3.1).

Installing the four residues, Y38W, A75D, I79Y and F133W, as single mutants onto ELIC decreased cysteamine potency, whilst maintaining the inhibitory function of ACh. Initially, ELIC was postulated to be activated by ACh, due to the conserved aromatic residues in the orthosteric site that surround a pocket similar in volume to the nAChR (Hilf and Dutzler, 2008). Subsequently, in 2012, Pan et al. identified that ACh binds in this very pocket with the same binding pose as primary amines, but instead competitively antagonizes the agonist-induced response. One of our mutations, F133W, presents a tryptophan, which has previously been well-characterized in the nAChRs. The homologous αW149, in the muscle-type nAChR, and W143, in *Ls*-AChBP, is considered one of the most critical aromatic position for strong cation-π interactions with the choline head group of ACh (Zhong et al., 1998; Olsen et al., 2014). By inserting a bulky and electron-rich tryptophan, we expected to increase ACh binding affinity, which would in turn increase the potency of ACh inhibition or convert ACh into an agonist. Instead, F133W resulted in a 7-fold and 10-fold decrease in cysteamine $EC_{50}$ and ACh $IC_{50}$ respectively, which suggests that the tryptophan residue may not be oriented for optimal cation-π interaction in ELIC. In the muscle-type nAChR, the reciprocal mutation, αW149F, at this position decreases the receptor affinity of ACh 12-fold and channel opening rate constant by 93-fold (Gustav Akk, 2001). The second mutation that was installed is Y38W, which introduces

another highly conserved tryptophan in the nAChR subfamily (Karlin, 2002; Olsen et al., 2014). This tryptophan residue, known in the muscle-type nAChR as γW55/δW57, is a central agonist contact on the complementary subunit interface (Olsen et al., 2014). Mutating the homologous tryptophan residue to an alanine in the α4β2 nAChR disrupts ACh gating, which, in the *Ls*-AChBP, is shown to form a cation-π interaction with the choline head group of ACh (Olsen et al., 2014). In ELIC, Y38W results in no significant shift in potency of cysteamine or ACh. A third aromatic installation was done with the mutation I79Y. Isoleucine is suggested to form Van der Waals contacts with the aliphatic carbon atoms of ELIC agonists (Zimmermann and Dutlzer, 2011). The resulting tyrosine residue is highly conserved in the nAChR subfamily and functions as a hydrogen bond donor in AChBPs and the α7-AChBP chimaera, stabilizing the quaternary amine head group of the ligand (Li et al., 2011; Olsen et al., 2014). Surprisingly, inserting this tyrosine, which was expected to form a hydrogen bond to stabilize ACh and cysteamine binding, resulted in the largest decrease in cysteamine potency of any single mutation. A very slow activating and/or slow desensitizing channel was produced, with at least a 24-fold decrease in cysteamine potency. A possible rationale involves residue E131, which forms electrostatic interactions with both agonists and ACh at the amine group (Zimmermann and Dutzler, 2011; Pan et al., 2012). Residue E131 also undergoes a significant conformational change upon ACh binding in ELIC and corresponds to the conserved β2-E155 in $GABA_A$ receptors, which is involved in linking agonist binding to channel gating (Newell et al., 2004; Pan et al., 2012). In the nAChR subfamily and AChBP, this E131 residue is a conserved glycine, which was also identified in the red sector (Appendix Figure 4.1). E131 was not selected for mutagenesis due to the electrostatic interaction it forms with ACh and agonists in ELIC, which we hoped to maintain for high affinity binding. It appears that in the ACh-ELIC crystal structure, residue E131 is

proximal to I79, which, upon mutation to the bulkier tyrosine, may result in a clash between the two residues (Figure 1.6B). This tyrosine, as a result, may be disrupting E131 signal transduction. Additionally, E131 may be disrupting Y79 from forming a hydrogen bond with the agonist, ultimately manifesting in the phenotype we observe for the I79Y mutant. The last position that was mutated is position 75, which is an alanine located in the second shell of residues away from the orthosteric site; this had not been previously implicated in agonism of ELIC. The homologous position in AChBPs and nAChRs is an aspartic acid that, upon mutation to an asparagine, slows ACh binding without affecting signal transduction of the muscle-type nAChR (Lee and Sine, 2004). This distal aspartic acid residue in the muscle-type nAChR influences ACh binding by forming a hydrogen bond with the main chain amide of αW149, positioning this tryptophan for optimal cation-π interactions with ACh (Lee and Sine, 2004). Characterizing this A75D mutation in ELIC resulted in a roughly 3-fold decrease in cysteamine potency, highlighting the importance of this position for agonism. Out of any single mutant, this distal A75D mutation had the largest decrease in ACh potency, of roughly 10-fold. It is possible that A75D is influencing both cysteamine and ACh binding through a similar mechanism to the muscle-type nAChR. D75 may be interacting with F133, which is homologous to αW149, and positioning the aromatic ring in a different orientation and distance from the two ligands. However, unlike the muscle-type nAChR, this new orientation and/or distance of the aromatic ring is hindering ACh and cysteamine contact.

Installing the A75D/F133W double mutant onto ELIC abolished ACh's antagonist activity, and instead converted ACh into a potentiator of agonist-activated currents. The A75D/F133W double mutant is of particular interest because these two mutations recapitulate the key residues that are present in the muscle-type nAChR, αD85 and αW149. As mentioned in

the nAChR and AChBP, these two residues interact through a hydrogen bond with the aspartic acid, positioning tryptophan in an optimal orientation for high affinity ACh binding. A roughly additive decrease in cysteamine potency was observed when these two mutants are combined, with a modest 12-fold change compared to WT. These two residues must be functionally interacting in ELIC, because they abolish ACh's function as an inhibitor. In the absence of any functional interaction, the ACh potency would decrease by 100-fold, given that A75D and F133W individually decrease the potency by roughly 10-fold each. In this case, we would observe significant inhibition at concentrations as high as 100 mM of ACh; instead, in practice, what we found at this concentration was the highest level of potentiation (Figure 3.4C). The new function that is created in the A75D/F133W double mutant upon ACh binding appears to be potentiation, instead of agonism.

Several mechanisms could explain the observed potentiation. Potentiation is seen with high ACh concentration such as 25 mM, 50 mM and 100 mM (Figure 3.4C, Figure 3.5A, Figure 3.6). In the absence of ACh binding to ELIC, all of these cationic ACh molecules reside in the buffer/extracellular environment of the oocyte, contributing to the Nernst potential of the permeant ions, such as calcium and sodium. The running buffer contains 150 mM NaCl and 0.5 mM $BaCl_2$; thus, 25 mM or 100 mM of ACh can be considered a relatively substantial amount of cations. In the absence of receptor binding, all of these ACh molecules may be increasing the driving force of sodium ions through ELIC (i.e. contributing to the sodium equilibrium potential). Alternatively, ACh may be directly potentiating cysteamine-induced ELIC currents by binding to the orthosteric site. Evidence for a direct mechanism arises from that fact that we see a different degree of ACh-driven potentiation depending on the concentration of cysteamine present. Highest levels of potentiation from 25 mM ACh occur near cysteamine saturation,

whilst less potentiation is seen at the $EC_{10}$ of cysteamine. If this was purely due to changes in the sodium equilibrium potential, the magnitude of the effect would not depend upon the concentration of cysteamine. Upon binding cysteamine, channels transition from a resting to an active/open conformation, as well as a desensitized conformation, in which agonist is bound, but ions cannot permeate the receptor. The rate of desensitization is cysteamine concentration-dependent, with faster desensitization occurring at higher cysteamine concentrations. The difference in rate of desensitization can be seen on a TEVC trace as the steepness of the upward deflection after a peak current is reached. Desensitization also decreases the magnitude of the peak current, which is most clearly visible at very high cysteamine concentrations (Figure 3.2A). It is possible that upon binding of ACh, the rate of desensitization of the cysteamine-activated channels is slowed. This would explain why, at higher cysteamine concentrations, with the fastest rate of desensitization, we see the largest amount of potentiation by ACh.

Structurally, ACh may be binding in the agonist binding site to alter ELIC desensitization. The agonist binding site can accommodate more than one ligand in the nAChR and AChBP due to the flexibility of the C-loop (Brams et al., 2011; Stornaiuolo et al., 2013). An extreme example of this is the binding of VUF9432, an aromatic small molecule, to the AChBP, as an ordered π-π stack of three identical molecules per binding site (Stornaiuolo et al., 2013). Another example is the binding of two acetylcholine molecules in a single agonist binding site of the modified *Apylsia* AChBP (Brams et al., 2011). It is thus plausible that ACh, along with cysteamine, are occupying the same binding site, in which the additional contacts offered by ACh are stabilizing the open state of the receptor or destabilizing the resting/desensitized conformations. Alternatively, ACh might be binding to agonist binding sites that are unoccupied by cysteamine. Homopentameric proteins such as ELIC contain five agonist binding sites, where

cysteamine may only occupy a fraction of these sites to achieve full channel activation. This leaves the remaining unoccupied agonist binding sites as possible ACh targets, resulting in the observed potentiation.

In 2012, Pan et al. suggested that ELIC is on the verge of activation when bound by ACh. To support this, they replaced a single methyl group of ACh by a hydrogen, yielding the DMAEA molecule, which was able to activate the receptor. Consequently, stronger interactions with ACh at this choline head group should be able to activate the receptor. By making small structural perturbations to enhance interaction with the quaternary amine of ACh, we found that installing ACh agonism in ELIC is complicated. There are 15 residues that differ between homologous positions in ELIC and the AChBP red sector, of which we have only tested four. A possible shortcoming of focusing solely on these four residues is that the other 11 residues may contain ELIC residues that are not compatible and/or interfere with ACh agonism. One of these residues out of the 11 is E131, which, as mentioned, may be clashing with Y79. This clash could be alleviated by incorporating the mutation E131G, as the red sector glycine in AChBP is highly conserved in nAChRs as well. Another residue that may be preventing ACh agonism in ELIC is E129, which is homologous to α1K145 in the muscle-type nAChR. The α1K145 residue is involved in relaying the initial conformational changes upon ACh binding towards channel gating (Mukhtasimova et al., 2005). The idea of having incompatible background residues from the red sector in ELIC is consistent with what we see in terms of cysteamine potency. By installing residues that are key for ACh agonism in nAChRs, we decrease cysteamine potency in ELIC. The decreased potency is surprising, because all the mutations offer more electron-rich groups for stronger interaction with the primary amine region of cysteamine. Mutants such as I79Y or F133W may be clashing or oriented differently, due to incompatible background

residues that are interfering with optimal agonist contact. The converse is also true in the muscle-type nAChR; the mutant W149F, which installs the ELIC F133 residue, decreases ACh affinity and channel opening rate, as phenylalanine is not optimized for agonism in the background of muscle-type nAChR residues. In order to change agonist specificity, we must consider compensatory mutations and the entire sequence of residues that constitutes a sector. It will be interesting to test whether ACh agonism can be installed through transplantation of the nAChR residues within the entire red sector into ELIC.

None of the mutants were activated by ACh, but we cannot rule out the possibility that ACh is binding with higher affinity. Using TEVC electrophysiology, we are measuring a channel response, which is the magnitude of current conducted through ELIC in the presence of different ligand concentrations. This measurement of ligand potency involves ligand binding and channel gating. For this reason, we cannot distinguish between decreased potency caused by less efficient channel gating and/or by weakened ligand binding affinity. To determine the ACh binding affinity and identify if ACh is directly potentiating the A75D/F133W double mutant cysteamine currents, a future experiment with the α-bungarotoxin inhibitor will be performed. By installing an $^{125}$I-labelled α-bungarotoxin ($^{125}$I-BTX) binding epitope onto ELIC, which has been previously done for the prokaryotic GLIC receptor, a competitive binding assay between ACh and $^{125}$I-BTX can be performed (Vincent et al., 1998; Wang et al., 2011). If ACh is not directly binding to the orthosteric site of ELIC, we would expect no significant change in $^{125}$I-BTX binding when ACh concentrations are increased in the presence of a fixed $^{125}$I-BTX concentration. Another experiment that can be performed to tease apart the direct vs indirect mechanism of ACh potentiation is to determine the $EC_{50}$ of cysteamine, in the presence of a fixed ACh concentration. In the A75D/F133W mutant, if ACh is directly potentiating

cysteamine-induced ELIC currents, we should see a decrease in the $EC_{50}$ of cysteamine in the presence of ACh (Ruesch et al., 2012). In contrast, the presence of a fixed ACh concentration shifts the cysteamine $EC_{50}$ to higher values for the WT ELIC receptor (Pan et al., 2012).

In conclusion, this study demonstrates the utility of using SCA to identify functionally important residues for pLGIC agonism. By converting ACh from an inhibitor to a potentiator with the A75D/F133W ELIC double mutant, we show that a synthetic approach can be used with pLGICs to alter function between a ligand and a receptor. Due to epistatic interactions, the entire group of residues comprising a sector, or select residues within a sector that are distant from the ligand-binding site, need to be considered in future efforts to install agonism. With the advent of new high-resolution cryo-EM structures of the full nAChR, SCA will be carried out on these receptors to unveil residues outside of the ECD that are key for ACh agonism.

# References

Akk, G. (2001) Aromatics at the murine nicotinic receptor agonist binding site: Mutational analysis of the αY93 and αW149 residues. *J. Physiol. 535*, 729–740

Alexander, S., Mathie, A., and Peters, J. (2011) LIGAND-GATED ION CHANNELS. *Br. J. Pharmacol. 164*, S115–S135

Andersen, N., Corradi, J., Sine, S. M., and Bouzat, C. (2013) Stoichiometry for activation of neuronal α7 nicotinic receptors. *Proc. Natl. Acad. Sci. U. S. A. 110*, 20819–20824

Beckstein, O., and Sansom, M. S. P. (2006) A Hydrophobic Gate in an Ion Channel: The Closed State of the Nicotinic Acetylcholine Receptor. *Phys. Biol. 3,* 147-159

Bocquet, N., Prado De Carvalho, L., Cartaud, J., Neyton, J., Le Poupon, C., Taly, A., Grutter, T., Changeux, J. P., and Corringer, P. J. (2007) A prokaryotic proton-gated ion channel from the nicotinic acetylcholine receptor family. *Nature 445*, 116–119

Bocquet, N., Nury, H., Baaden, M., Le Poupon, C., Changeux, J. P., Delarue, M., and Corringer, P. J. (2009) X-ray structure of a pentameric ligand-gated ion channel in an apparently open conformation. *Nature 457*, 111–114

Bouzat, C., Gumilar, F., Spitzmaul, G., Wang, H. L., Rayes, D., Hansen, S. B., Taylor, P., and Sine, S. M. (2004) Coupling of agonist binding to channel gating in an ACh-binding protein linked to an ion channel. *Nature 430*, 896–900

Bouzat, C., Bartos, M., Corradi, J., and Sine, S. M. (2008) The interface between extracellular and transmembrane domains of homomeric Cys-loop receptors governs open-channel lifetime and rate of desensitization. *J. Neurosci. 28*, 7808–7819

Brams, M., Gay, E. A., Sáez, J. C., Guskov, A., Van Elk, R., Van Der Schors, R. C., Peigneur, S., Tytgat, J., Strelkov, S. V., Smit, A. B., Yakel, J. L., and Ulens, C. (2011) Crystal structures of a cysteine-modified mutant in loop D of acetylcholine-binding protein. *J. Biol. Chem. 286*, 4420–4428

Breckenridge, R. J., Nicholson, S. H., Nicol, A. J., Suckling, C. J., Leigh, B., and Iversen, L. (1981) Inhibition of [3H]GABA Binding to Postsynaptic Receptors in Human Cerebellar Synaptic Membranes by Carboxyl and Amino Derivatives of GABA. *J. Neurochem. 37*, 837–844

Brejc, K., Van Dijk, W. J., Klaassen, R. V., Schuurmans, M., Van Der Oost, J., Smit, A. B., and Sixma, T. K. (2001) Crystal structure of an ACh-binding protein reveals the ligand-binding domain of nicotinic receptors. *Nature 411*, 269–276

Burzomato, V., Beato, M., Groot-Kormelink, P. J., Colquhoun, D., and Sivilotti, L. G. (2004) Single-channel behavior of heteromeric α1β glycine receptors: An attempt to detect a conformational change before the channel opens. *J. Neurosci. 24*, 10924–10940

Carter, P. J., Winter, G., Wilkinson, A. J., and Fersht, A. R. (1984) The use of double mutants to detect structural changes in the active site of the tyrosyl-tRNA synthetase (Bacillus stearothermophilus). *Cell 38*, 835–840

Celie, P. H. N., Kasheverov, I. E., Mordvintsev, D. Y., Hogg, R. C., Van Nierop, P., Van Elk, R., Van Rossum-Fikkert, S. E., Zhmak, M. N., Bertrand, D., Tsetlin, V., Sixma, T. K., and Smit, A. B. (2005) Crystal structure of nicotinic acetylcholine receptor homolog AChBP in complex with an α-conotoxin PnIA variant. *Nat. Struct. Mol. Biol. 12*, 582–588

Chang, C. C., and Lee, C. Y. (1963) Isolation of Neurotoxins from the Venom of Bungarus Multicinctus and Their Modes of Neuromuscular Blocking Action. *Arch. Int. Pharmacodyn. Ther. 144,* 241-257

Corringer, P. J., Bertrand, S., Galzi, J. L., Devillers-Thiéry, A., Changeux, J. P., and Bertrand, D. (1999) Mutational analysis of the charge selectivity filter of the α7 nicotinic acetylcholine receptor. *Neuron 22*, 831–843

daCosta, C. J. B., and Baenziger, J. E. (2009) A lipid-dependent uncoupled conformation of the acetylcholine receptor. *J. Biol. Chem. 284*, 17819–17825

daCosta, C. J. B., and Baenziger, J. E. (2013) Gating of pentameric ligand-gated ion channels: Structural insights and ambiguities. *Structure* 21, 1271-1283

Dellisanti, C. D., Yao, Y., Stroud, J. C., Wang, Z. Z., and Chen, L. (2007) Crystal structure of the extracellular domain of nAChR α1 bound to α-bungarotoxin at 1.94 Å resolution. *Nat. Neurosci. 10*, 953–962

Dellisanti, C. D., Yao, Y., Stroud, J. C., Wang, Z. Z., and Chen, L. (2007) Structural determinants for alpha-neurotoxin sensitivity in muscle nAChR and their implications for the gating mechanism. *Channels (Austin). 1*, 234–237

Dionisio, L., Bergé, I., Bravo, M., Del Carmen Esandi, M., and Bouzat, C. (2015) Neurotransmitter GABA activates muscle but not α7 nicotinic receptors. *Mol. Pharmacol. 87*, 391–400

Edelstein, S. J., Schaad, O., Henry, E., Bertrand, D., and Changeux, J. P. (1996) A kinetic mechanism for nicotinic acetylcholine receptors based on multiple allosteric transitions. *Biol. Cybern. 75*, 361–379

Ferguson, A. D., Amezcua, C. A., Halabi, N. M., Chelliah, Y., Rosen, M. K., Ranganathan, R., and Deisenhofer, J. (2007) Signal transduction pathway of TonB-dependent transporters. *Proc. Natl. Acad. Sci. U. S. A. 104*, 513–518

Fersht, A. R., Matouschek, A., and Serrano, L. (1992) The folding of an enzyme. I. Theory of protein engineering analysis of stability and pathway of protein folding. *J. Mol. Biol. 224*, 771–782

Gallivan, J. P., and Dougherty, D. A. (1999) Cation-π interactions in structural biology. *Proc. Natl. Acad. Sci. U. S. A. 96*, 9459–9464

Gunthorpe, M. J., and Lummis, S. C. R. (2001) Conversion of the Ion Selectivity of the 5-HT3A Receptor from Cationic to Anionic Reveals a Conserved Feature of the Ligand-gated Ion Channel Superfamily. *J. Biol. Chem. 276*, 10977–10983

Halabi, N., Rivoire, O., Leibler, S., and Ranganathan, R. (2009) Protein Sectors: Evolutionary Units of Three-Dimensional Structure. *Cell 138,* 774-786

Halavaty, A. S., and Moffat, K. (2007) N- and C-terminal flanking regions modulate light-induced signal transduction in the LOV2 domain of the blue light sensor phototropin 1 from Avena sativa. *Biochemistry 46*, 14001–14009

Hansen, S. B., Sulzenbacher, G., Huxford, T., Marchot, P., Taylor, P., and Bourne, Y. (2005) Structures of Aplysia AChBP complexes with nicotinic agonists and antagonists reveal distinctive binding interfaces and conformations. *EMBO J. 24*, 3635–3646

Hatley, M. E., Lockless, S. W., Gibson, S. K., Gilman, A. G., and Ranganathan, R. (2003) Allosteric determinants in guanine nucleotide-binding proteins. *Proc. Natl. Acad. Sci. U. S. A. 100*, 14445–14450

Heidmann, T., and Changeux, J. P. (1978) Structural and Functional Properties of the Acetylcholine Receptor Protein in its Purified and Membrane-Bound States. *Annu. Rev. Biochem. 47*, 317–357

Heidmann, T., and Changeux, J. P. (1980) Interaction of a fluorescent agonist with the membrane-bound acetylcholine receptor from Torpedo marmorata in the millisecond time range: Resolution of an “intermediate” conformational transition and evidence for positive cooperative effects. *Biochem. Biophys. Res. Commun. 97*, 889–896

Hidalgo, P., and MacKinnon, R. (1995) Revealing the architecture of a K+ channel pore through mutant cycles with a peptide inhibitor. *Science 268*, 307–310

Hilf, R. J. C., and Dutzler, R. (2008) X-ray structure of a prokaryotic pentameric ligand-gated ion channel. *Nature 452*, 375–379

Hilf RJ, Dutzler R (2009) A prokaryotic perspective on pentameric ligand-gated ion channel structure. *Curr Opin Struct Biol 19*, 418–424

Hilf, R. J. C., and Dutzler, R. (2009) Structure of a potentially open state of a proton-activated pentameric ligand-gated ion channel. *Nature 457*, 115–118

Huang, S., Li, S. X., Bren, N., Cheng, K., Gomoto, R., Chen, L., and Sine, S. M. (2013) Complex between α-bungarotoxin and an α7 nicotinic receptor ligand-binding domain chimaera. *Biochem. J. 454*, 303–310

Imoto, K., Busch, C., Sakmann, B., Mishina, M., Konno, T., Nakai, J., Bujo, H., Mori, Y., Fukuda, K., and Numa, S. (1988) Rings of negatively charged amino acids determine the acetylcholine receptor channel conductance. *Nature 335*, 645–648

Ivanov, I., Cheng, X., Sine, S. M., and McCammon, J. A. (2007) Barriers to ion translocation in cationic and anionic receptors from the cys-loop family. *J. Am. Chem. Soc. 129*, 8217–8224

Jackson, M. B. (1984) Spontaneous openings of the acetylcholine receptor channel. *Proc. Natl. Acad. Sci. U. S. A. 81*, 3901–3904

Kao, P.N., Karlin, A. (1986). Acetylcholine receptor binding site contains a disulfide cross-link between adjacent half-cystinyl residues. *J. Biol. Chem. 261,* 8085-8088

Karlin, A. (2002) Ion channel structure: Emerging structure of the Nicotinic Acetylcholine receptors. *Nat. Rev. Neurosci. 3*, 102–114

Kelley, S. P., Dunlop, J. I., Kirkness, E. F., Lambert, J. J., and Peters, J. A. (2003) A cytoplasmic region determines single-channel conductance in 5-HT3 receptors. *Nature 424*, 321–324

Keramidas, A., Moorhouse, A. J., Schofield, P. R., and Barry, P. H. (2004) Ligand-gated ion channels: Mechanisms underlying ion selectivity. *Prog. Biophys. Mol. Biol. 86,* 161-204

Keramidas, A., and Lynch, J. W. (2013) An outline of desensitization in pentameric ligand-gated ion channel receptors. *Cell. Mol. Life Sci. 70*, 1241–1253

Koshland, D. E. (1959) Enzyme flexibility and enzyme action. *J. Cell. Comp. Physiol. 54*, 245–258

Krashia, P., Lape, R., Lodesani, F., Colquhoun, D., and Sivilotti, L. G. (2011) The long activations of α2 glycine channels can be described by a mechanism with reaction intermediates ("flip"). *J. Gen. Physiol. 137*, 197–216

Laitko, U., Juranka, P. F., and Morris, C. E. (2006) Membrane stretch slows the concerted step prior to opening in a Kv channel. *J. Gen. Physiol. 127*, 687–701

Lape, R., Colquhoun, D., and Sivilotti, L. G. (2008) On the nature of partial agonism in the nicotinic receptor superfamily. *Nature 454*, 722–727

Lasalde, J. A., Tamamizu, S., Butler, D. H., Vibat, C. R. T., Hung, B., and McNamee, M. G. (1996) Tryptophan substitutions at the lipid-exposed transmembrane segment M4 of Torpedo californica acetylcholine receptor govern channel gating. *Biochemistry 35*, 14139–14148

Lee, W. Y., and Sine, S. M. (2004) Invariant aspartic acid in muscle nicotinic receptor contributes selectively to the kinetics of agonist binding. *J. Gen. Physiol. 124*, 555–567

Lee, W. Y., and Sine, S. M. (2005) Principal pathway coupling agonist binding to channel gating in nicotinic receptors. *Nature 438*, 243–247

Lee, W.Y., Free, C.R., and Sine, S.M. (2008). Nicotinic receptor interloop proline anchors beta1-beta2 and Cys loops in coupling agonist binding to channel gating. *J. Gen. Physiol. 132*, 265-278

Lee, J., Natarajan, M., Nashine, V. C., Socolich, M., Vo, T., Russ, W. P., Benkovic, S. J., and Ranganathan, R. (2008) Surface sites for engineering allosteric control in proteins. *Science 322*, 438–442

Li, S. X., Huang, S., Bren, N., Noridomi, K., Dellisanti, C. D., Sine, S. M., and Chen, L. (2011) Ligand-binding domain of an α7-nicotinic receptor chimera and its complex with agonist. *Nat. Neurosci. 14*, 1253–1259

Lockless, S. W., and Ranganathan, R. (1999) Evolutionarily conserved pathways of energetic connectivity in protein families. *Science 286*, 295–299

Marabelli, A., Lape, R., and Sivilotti, L. (2015) Mechanism of activation of the prokaryotic channel ELIC by propylamine: A single-channel study. *J. Gen. Physiol. 145*, 23–45

Marinou, M., and Tzartos, S. J. (2003) Identification of regions involved in the binding of α-bungarotoxin to the human α7 neuronal nicotinic acetylcholine receptor using synthetic peptides. *Biochem. J. 372*, 543–554

Martínez-Castilla, L. P., and Rodríguez-Sotres, R. (2010) A Score of the Ability of a Three-Dimensional Protein Model to Retrieve Its Own Sequence as a Quantitative Measure of Its Quality and Appropriateness. *PLoS One* (Haslam, N. J., Ed.) *5*, e12483

McLaughlin, R. N., Poelwijk, F. J., Raman, A., Gosal, W. S., and Ranganathan, R. (2012) The spatial architecture of protein function and adaptation. *Nature 491*, 138–142

Miller, P. S., and Smart, T. G. (2010) Binding, activation and modulation of Cys-loop receptors. *Trends Pharmacol. Sci. 31,* 161-174

Miyazawa, A., Fujiyoshi, Y., Stowell, M., and Unwin, N. (1999) Nicotinic acetylcholine receptor at 4.6 Å resolution: Transverse tunnels in the channel wall. *J. Mol. Biol. 288*, 765–786

Miyazawa, A., Fujiyoshi, Y., and Unwin, N. (2003) Structure and gating mechanism of the acetylcholine receptor pore. *Nature 423*, 949–955

Monod, J., Wyman, J., and Changeux, J. P. (1965) On the nature of allosteric transitions: A plausible model. *J. Mol. Biol. 12*, 88–118

Morlock, E. V., and Czajkowski, C. (2011) Different residues in the GABAA receptor benzodiazepine binding pocket mediate benzodiazepine efficacy and binding. *Mol. Pharmacol. 80*, 14–22

Mukhtasimova, N., Free, C., and Sine, S. M. (2005) Initial coupling of binding to gating mediated by conserved residues in the muscle nicotinic receptor. *J. Gen. Physiol. 126*, 23–39

Mukhtasimova, N., Lee, W. Y., Wang, H. L., and Sine, S. M. (2009) Detection and trapping of intermediate states priming nicotinic receptor channel opening. *Nature 459*, 451–454

Newell, J. G., McDevitt, R. A., and Czajkowski, C. (2004) Mutation of glutamate 155 of the GABAA receptor β2 subunit produces a spontaneously open channel: A trigger for channel activation. *J. Neurosci. 24*, 11226–11235

Olsen, J. A., Balle, T., Gajhede, M., Ahring, P. K., and Kastrup, J. S. (2014) Molecular recognition of the neurotransmitter acetylcholine by an acetylcholine binding protein reveals determinants of binding to nicotinic acetylcholine receptors. *PLoS One 9,* e91232

Pan, J., Chen, Q., Willenbring, D., Yoshida, K., Tillman, T., Kashlan, O. B., Cohen, A., Kong, X. P., Xu, Y., and Tang, P. (2012) Structure of the pentameric ligand-gated ion channel ELIC cocrystallized with its competitive antagonist acetylcholine. *Nat. Commun. 3*, 1–8

Purohit, P., and Auerbach, A. (2009) Unliganded gating of acetylcholine receptor channels. *Proc. Natl. Acad. Sci. U. S. A. 106*, 115–120

Rahman, M. M., Teng, J., Worrell, B. T., Noviello, C. M., Lee, M., Karlin, A., Stowell, M. H. B., and Hibbs, R. E. (2020) Structure of the Native Muscle-type Nicotinic Receptor and Inhibition by Snake Venom Toxins. *Neuron. 106,* 1-11

Rollema H., Bertrand D., Hurst R.S. (2010) Nicotinic Agonists and Antagonists. In: Stolerman I.P. (eds) Encyclopedia of Psychopharmacology. Springer, Berlin, Heidelberg

Ruesch, D., Neumann, E., Wulf, H., and Forman, S. A. (2012) An allosteric coagonist model for propofol effects on α1β 2γ2L γ-Aminobutyric acid type A receptors. *Anesthesiology 116*, 47–55

Russ, W. P., Lowery, D. M., Mishra, P., Yaffe, M. B., and Ranganathan, R. (2005) Natural-like function in artificial WW domains. *Nature 437*, 579–583

Sakmann, B., Patlak, J., and Neher, E. (1980) Single acetylcholine-activated channels show burst-kinetics in presence of desensitizing concentrations of agonist. *Nature 286*, 71–73

Salinas, V. H., and Ranganathan, R. (2018) Coevolution-based inference of amino acid interactions underlying protein function. *eLife 7*, e34300

Schmieden, V., and Betz, H. (1995) Pharmacology of the inhibitory glycine receptor: agonist and antagonist actions of amino acids and piperidine carboxylic acid compounds. *Mol. Pharmacol. 48*, 919–927

Shulman, A. I., Larson, C., Mangelsdorf, D. J., and Ranganathan, R. (2004) Structural determinants of allosteric ligand activation in RXR heterodimers. *Cell 116*, 417–429

Silva, D., Santos, G., Barroca, M., and Collins, T. (2017) Inverse PCR for point mutation introduction. *Methods in Molecular Biology. 1620*, 87–100

Sivilotti, L. G. (2010) What single-channel analysis tells us of the activation mechanism of ligand-gated channels: The case of the glycine receptor. *J. Physiol. 588,* 45-58

Smit, A. B., Syed, N. I., Schaap, D., Van Minnen, J., Klumperman, J., Kits, K. S., Lodder, H., Van Der Schors, R. C., Van Elk, R., Sorgedrager, B., Brejc, K., Sixma, T. K., and Geraerts, W. P. M. (2001) A glia-derived acetylcholine-binding protein that modulates synaptic transmission. *Nature 411*, 261–268

Smock, R. G., and Gierasch, L. M. (2009) Sending signals dynamically. *Science 324,* 198-203

Spurny, R., Ramerstorfer, J., Price, K., Brams, M., Ernst, M., Nury, H., Verheij, M., Legrand, P., Bertrand, D., Bertrand, S., Dougherty, D. A., de Esch, I. J. P., Corringer, P.-J., Sieghart, W., Lummis, S. C. R., and Ulens, C. (2012) Pentameric ligand-gated ion channel ELIC is activated by GABA and modulated by benzodiazepines. *Proc. Natl. Acad. Sci. 109,* E3028-E3034

Stornaiuolo, M., De Kloe, G. E., Rucktooa, P., Fish, A., Van Elk, R., Edink, E. S., Bertrand, D., Smit, A. B., De Esch, I. J. P., and Sixma, T. K. (2013) Assembly of a π-π Stack of ligands in the binding site of an acetylcholine-binding protein. *Nat. Commun. 4, 1875*

Sun, J., Comeau, J. F., and Baenziger, J. E. (2017) Probing the structure of the uncoupled nicotinic acetylcholine receptor. *Biochim. Biophys. Acta - Biomembr. 1859*, 146–154

Tasneem, A., Iyer, L. M., Jakobsson, E., and Aravind, L. (2005) Identification of the prokaryotic ligand-gated ion channels and their implications for the mechanisms and origins of animal Cys-loop ion channels. *Genome Biol. 6*, R4

Taylor, P., Talley, T. T., Radic', Z., Hansen, S. B., Hibbs, R. E., and Shi, J. (2007) Structure-guided drug design: Conferring selectivity among neuronal nicotinic receptor and acetylcholine-binding protein subtypes. *Biochem. Pharmacol. 74*, 1164–1171

Thompson, A. J., Lester, H. A., and Lummis, S. C. R. (2010) The structural basis of function in Cys-loop receptors. *Q. Rev. Biophys. 43*, 449–499

Thompson, A. J., Alqazzaz, M., Ulens, C., and Lummis, S. C. R. (2012) The pharmacological profile of ELIC, a prokaryotic GABA-gated receptor. *Neuropharmacology 63*, 761–767

Tillman, T. S., Seyoum, E., Mowrey, D. D., Xu, Y., and Tang, P. (2014) ELIC-7 Nicotinic Acetylcholine Receptor (7nAChR) Chimeras Reveal a Prominent Role of the Extracellular-Transmembrane Domain Interface in Allosteric Modulation. *Journal of Biological Chemistry 289,* 20

Unwin, N., Miyazawa, A., Li, J., and Fujiyoshi, Y. (2002). Activation of the nicotinic acetylcholine receptor involves a switch in conformation of the alpha subunits. *J. Mol. Biol. 319,* 1165-1176

Unwin N. (2005) Refined structure of the nicotinic acetylcholine receptor at 4 Å resolution. *J. Mol. Biol. 346,* 967–989

Vincent, A., Jacobson, L., and Curran, L. (1998) α-Bungarotoxin binding to human muscle acetylcholine receptor: Measurement of affinity, delineation of AChR subunit residues crucial to binding, and protection of AChR function by synthetic peptides. *Neurochem. Int. 32*, 427–433

Wang, G.K., Schmidt, J. (1980) Primary Structure and Binding Properties of Iodinated Derivatives of Alpha-Bungarotoxin. *J. Biol. Chem. 255*, 11156-62

Wang, H. L., Cheng, X., and Sine, S. M. (2012) Intramembrane proton binding site linked to activation of bacterial pentameric ion channel. *J. Biol. Chem. 287,* 6482-6489

Wang, M. De, Rahman, M., Zhu, D., Johansson, I. M., and Bäckström, T. (2007) 3β-hydroxysteroids and pregnenolone sulfate inhibit recombinant rat GABAA receptor through different channel property. *Eur. J. Pharmacol. 557*, 124–131

Xiu, X., Puskar, N. L., Shanata, J. A. P., Lester, H. A., and Dougherty, D. A. (2009) Nicotine binding to brain receptors requires a strong cation- interaction. *Nature 458*, 534–537

Yamodo, I. H., Chiara, D. C., Cohen, J. B., and Miller, K. W. (2010) Conformational changes in the nicotinic acetylcholine receptor during gating and desensitization. *Biochemistry 49*, 156–165

Zhong, W., Gallivan, J. P., Zhang, Y., Li, L., Lester, H. A., and Dougherty, D. A. (1998) From ab initio quantum mechanics to molecular neurobiology: A cation-π binding site in the nicotinic receptor. *Proc. Natl. Acad. Sci. U. S. A. 95*, 12088–12093

Zimmermann, I., and Dutzler, R. (2011) Ligand activation of the Prokaryotic Pentameric ligand-gated ion channel ELIC. *PLoS Biol. 9,* e1001101

Zimmermann, I., Marabelli, A., Bertozzi, C., Sivilotti, L. G., and Dutzler, R. (2012) Inhibition of the Prokaryotic Pentameric Ligand-Gated Ion Channel ELIC by Divalent Cations. *PLoS Biol 10,* p. e1001429

# Appendix

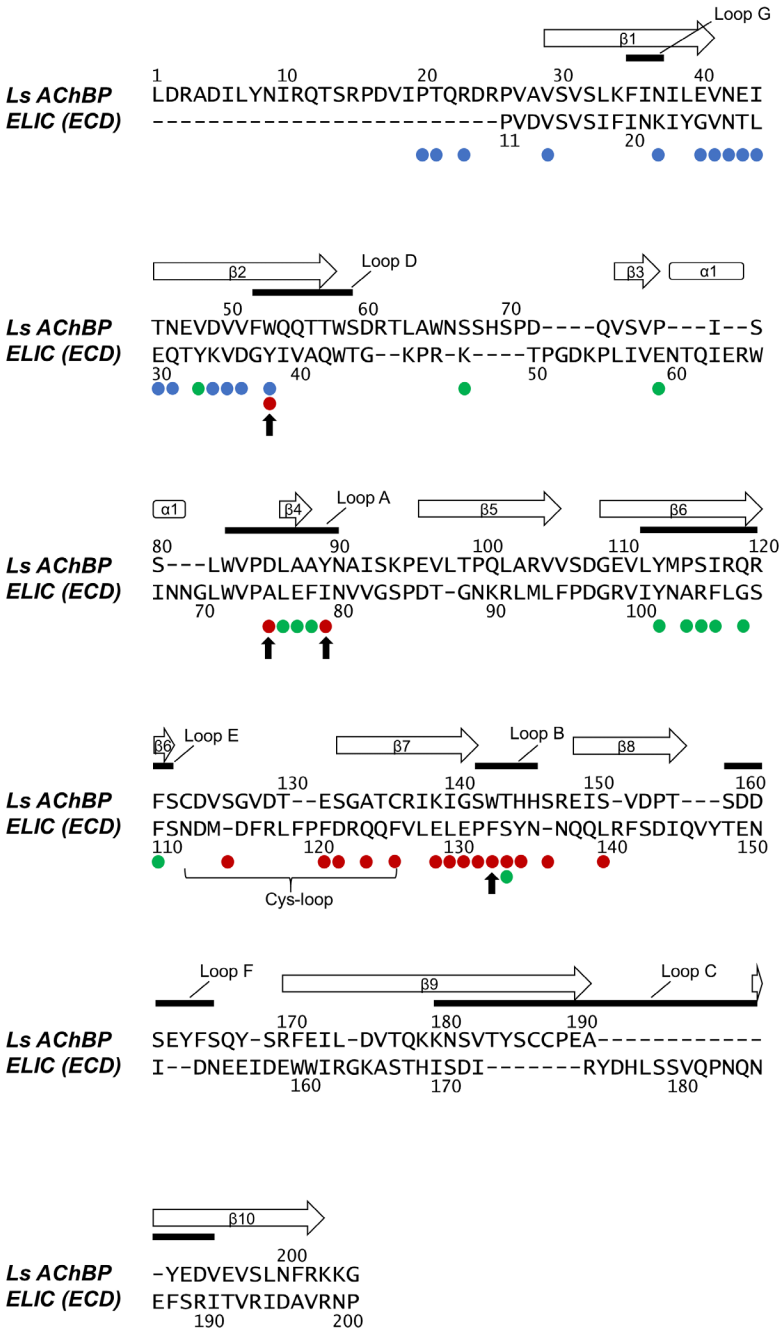


**Figure 4.1 Sequence alignment between *Ls*-AChBP and ELIC ECD**.

A structural alignment between the *Ls*-AChBP and ELIC ECD was done using the super algorithm in PyMOL. Secondary structure elements are indicated above the sequence with beta sheets, alpha helices and loops shown as arrows, rectangles, and bold lines respectively. The amino acid sequence numbers for AChBP (above) and ELIC (below) are highlighted. Blue, green and red sector positions are shown under the aligned sequence as coloured circles. A bold vertical arrow is used to indicate the four positions that were mutated in ELIC to install the homologous AChBP residues.

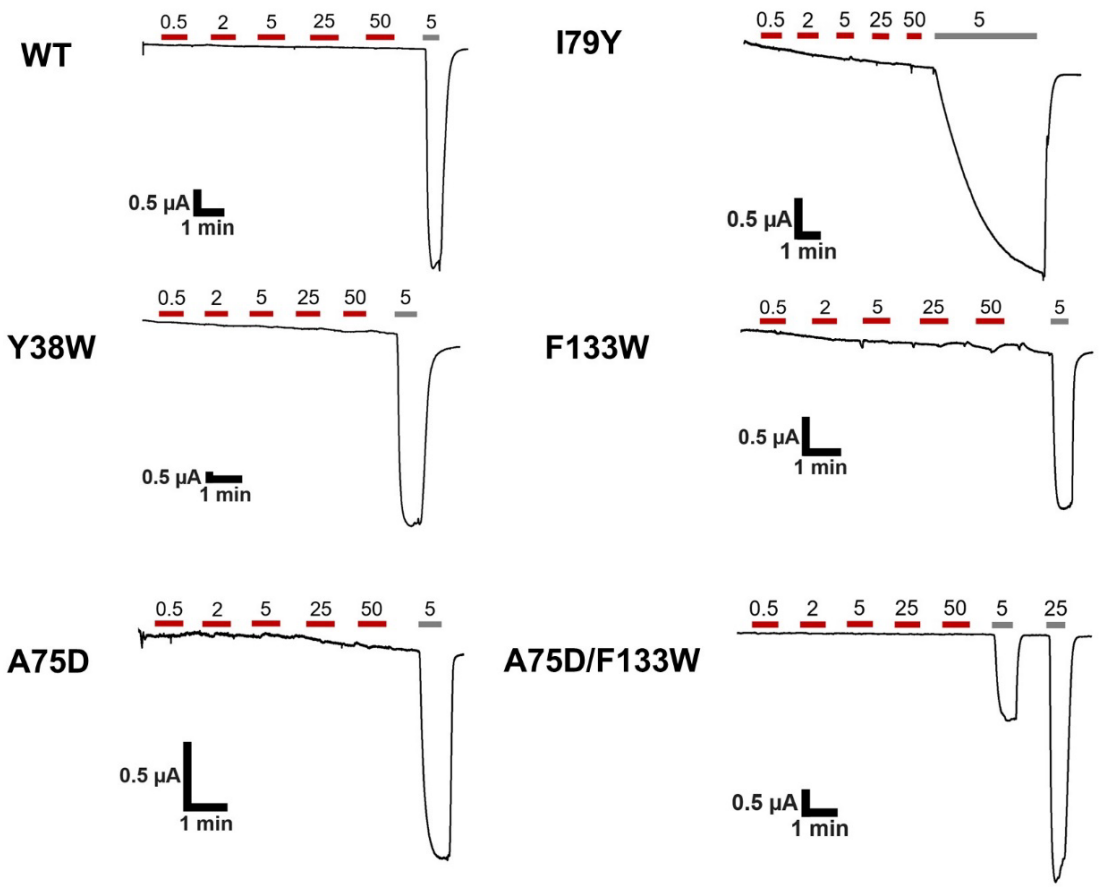


**Figure 4.2 Screening ACh and cysteamine ELIC channel activation.**

Representative whole cell TEVC traces are provided for each mutant and WT. The cysteamine or ACh concentrations (mM) that were used are indicated above each peak. The duration of cysteamine or ACh application is shown in gray bars and red bars respectively with the time in-between application representing a washing step that removes the ligand and returns channels to a baseline signal. A minimum of 3 oocytes were used from 2 batches to conclude that ACh does not activate ELIC.

**A**

***Ls* AChBP**

MRRNIFCLACLWIVQACLSLDRADILYNIRQTSRPDVIPTQRDRPVAVSVSLKF
INILEVNEITNEVDVVFWQQTTWSDRTLAWNSSHSPDQVSVPISSLWVPDLA
AYNAISKPEVLTPQLARVVSDGEVLYMPSIRQRFSCDVSGVDTESGATCRIKI
GSWTHHSREISVDPTTENSDDSEYFSQYSRFEILDVTQKKNSVTYSCCPEAY
EDVEVSLNFRKKGRSEIL

**B**

**pTLN – WT ELIC**

MGLRALMLWLLAAAGLVRESLSAPADNAADARPVDVSVSIFINKIYGVNTLEQ
TYKVDGYIVAQWTGKPRKTPGDKPLIVENTQIERWINNGLWVPALEFINVVGS
PDTGNKRLMLFPDGRVIYNARFLGSFSNDMDFRLFPFDRQQFVLELEPFSY
NNQQLRFSDIQVYTENIDNEEIDEWWIRGKASTHISDIRYDHLSSVQPNQNEF
SRITVRIDAVRNPSYYLWSFILPLGLIIAASWSVFWLESFSERLQTSFTLMLTV
VAYAFYTSNILPRLPYTTVIDQMIIAGYGSIFAAILLIIFAHHRQANGVEDDLLIQR
CRLAFPLGFLAIGCVLVIRGITL

ATGGGACTGAGAGCTCTGATGCTGTGGCTGCTGGCTGCTGCTGGACTGG
TGAGAGAATCTCTGAGTGCGCCGGCGGATAACGCGGCGGATGCCCGCC
CGGTGGATGTGAGTGTGAGCATTTTTATCAATAAGATCTACGGCGTGAACA
CGCTGGAGCAGACCTACAAGGTCGATGGCTACATCGTGGCGCAGTGGAC
CGGCAAACCGCGCAAAACGCCGGGCGATAAGCCATTGATTGTCGAAAAC
ACCCAGATCGAGCGGTGGATCAATAACGGATTATGGGTGCCGGCGCTGG
AATTCATCAACGTGGTCGGCAGCCCGGACACCGGCAATAAGCGCCTGAT
GCTGTTTCCCGACGGGCGGGTTATTTATAACGCCCGTTTTCTGGGCTCGT
TCAGCAATGACATGGACTTCCGGCTGTTTCCATTCGATCGTCAACAGTTC
GTGCTGGAACTGGAGCCTTTTTCCTATAACAACCAGCAACTGCGGTTCAG
CGATATACAGGTCTACACCGAGAATATTGATAACGAAGAGATCGACGAATG
GTGGATCCGGGGCAAAGCCTCGACCCACATCAGCGATATCCGTTACGAC
CATTTGAGCAGCGTGCAGCCCAATCAGAATGAGTTCTCCCGCATTACGGT
ACGGATCGACGCCGTTCGCAACCCGTCTTACTACCTGTGGAGTTTTATTC
TGCCGCTGGGGCTGATCATTGCCGCGTCATGGAGCGTGTTCTGGCTGGA
GTCTTTCTCCGAGCGTTTGCAGACCTCGTTCACCCTGATGCTGACGGTG
GTGGCCTATGCGTTTTACACCAGCAATATTCTGCCGCGGCTACCTTACACA
ACGGTCATCGACCAGATGATCATCGCCGGGTATGGCAGTATTTTCGCGGC
GATCCTACTGATTATTTTCGCCCACCACCGCCAGGCAAACGGCGTGGAG
GACGATCTGCTGATACAGCGCTGTCGTCTGGCCTTTCCTCTGGGGTTCCT
GGCGATCGGCTGCGTGCTGGTTATACGGGGGATTACACTATGA

**Figure 4.3 *Ls* AChBP amino acid sequence along with the open reading frame of ELIC with the α7 nAChR signal sequence.** (A) The *Ls* AChBP (Chain A) amino acid sequence was obtained from the 3WIP PDB FASTA file. (B) WT ELIC open reading frame DNA and amino acid sequence is provided, which begins with the α7 nAChR signal sequence (highlighted in cyan) followed by the ELIC coding sequence.